Absolute number of three populations of interneurons and all GABAergic synapses in the human hippocampus

Virág Takács[1, #], Péter Papp[1, #], Áron Orosz[1,2], Zsuzsanna Bardóczi[1], Tamás Zsoldos[1], Masahiko Watanabe[3], Zsófia Maglóczky[4], Péter Gombás[5], Tamás F. Freund[1], Gábor Nyiri[1,*]

[#] These authors contributed equally.
*Corresponding author. Email: nyiri@koki.hu

Affiliations:
1) Laboratory of Cerebral Cortex Research, Institute of Experimental Medicine, Budapest, Hungary
2) János Szentágothai Doctoral School of Neurosciences, Semmelweis University, Budapest, Hungary
3) Department of Anatomy and Embryology, Hokkaido University, Sapporo, Japan
4) Human Brain Research Laboratory, Institute of Experimental Medicine, Budapest, Hungary
5) Department of Pathology, St. Borbála Hospital, Tatabánya, Hungary

ABSTRACT

The human hippocampus plays a central role in learning and memory functions and is implicated in several neurological and psychiatric disorders linked to different subpopulations of its neurons. Understanding the complex workings of the human hippocampus requires computational models with accurate quantitative neuronal data. Although the total number of different hippocampal neurons and their synapses have been extensively described in rodents, most of these data are not available for the human hippocampus. All hippocampal functions are tightly regulated by different classes of local GABAergic interneurons. Therefore, here we used unbiased stereological methods to estimate the density and total number of three major GABAergic cell groups: the parvalbumin (PV)-expressing interneurons, the somatostatin (SOM)-positive interneurons and the calretinin (CR)-positive interneurons. We found that there are approximately 45600 PV-positive, 134500 SOM-positive and 228000 CR-positive interneurons per hippocampal hemisphere. Compared to rodent data, the higher proportion of CR-positive -typically interneuron selective- cells may contribute to a more robust regulation of local interneurons. We also used 3-dimensional electron microscopy to estimate the total number of GABAergic boutons and synapses in the different layers of the hippocampus, and we also quantified those originating from PV-positive neurons. We estimated that there are at least about $1.82 * 10^{10}$ GABAergic synapses in one hippocampal hemisphere, of which about $2.77 * 10^{9}$ are PV-positive, representing about 15.2% of the total GABAergic synapses of local or afferent neurons.

INTRODUCTION

Characterizing the structure, neuronal connections and ultimately the operating principles of the human hippocampus is essential for understanding its involvement in the formation, consolidation, and retrieval of memory traces, in supporting spatial navigation, in adaptive behaviors, and in various cognitive functions (Cai et al., 2016; Roy et al., 2017; Szőnyi et al., 2019; Goode et al., 2020; Zichó et al., 2023). These require computational models that are based on accurate data on the number of neurons in different neuronal classes, which are the cornerstone of any type of modeling (Brunton and Beyeler, 2019; Gandolfi et al., 2023).

Unfortunately, there are only a limited number of studies that have attempted to collect statistically reliable data on key quantitative parameters of the human hippocampus (West and Gundersen, 1990; Harding et al., 1998), and in particular, key GABAergic interneurons have hardly been studied. Recently, Gandolfi et al. proposed a full-scale scaffold model of the human hippocampal CA1 area (Gandolfi et al., 2023). The total number of cells within this volume was estimated to be 18 million, including glial cells and neurons. Based on the assumption that the cellular composition of human and rodent hippocampi is similar, they calculated that 5.28 million of these cells would be neurons, out of which 4.8 million would be principal cells and 0.48 million would be GABAergic interneurons. However, no direct estimate of the different subpopulations of interneurons has been published.

Different inhibitory interneuron subtypes in the human and rodent hippocampi project to different layers, providing functional segregation of inhibitory patterns (Freund and Buzsáki, 1996; Klausberger and Somogyi, 2008; Pelkey et al., 2017). Inhibitory cells of diverse origin and function exhibit distinct protein expression patterns, allowing the classification of hippocampal interneurons into subgroups based on specific molecular markers (Freund and Buzsáki, 1996; Klausberger and Somogyi, 2008; DeFelipe et al., 2013; Pelkey et al., 2017). A large subset of interneurons express the calcium-binding molecule parvalbumin (PV), and most of these cells preferentially innervate the perisomatic regions of principal cells: the cell body and the proximal dendrites [basket cells, (Katsumaru et al., 1988)] or the axon initial segments [axo-axonic cells; (Somogyi, 1977; Somogyi et al., 1982; DeFelipe et al., 1989)]. Expression of the neuropeptide somatostatin (SOM) can be detected in a significant proportion of dendrite-targeting interneurons, which preferentially target distal dendrites of principal cells (Kosaka et al., 1988; Klausberger, 2009; Honoré et al., 2021). A large population of interneurons produce another calcium-binding protein, calretinin. Many of these neurons are interneuron-selective interneurons that innervate other interneurons and thus can directly regulate inhibition within the hippocampus (Gulyás et al., 1996; Urbán et al., 2002; Tóth et al., 2010). These interneurons are ideally positioned to orchestrate the formation and reactivation of memory traces, to control the flow of information, and to establish and maintain hippocampal rhythms (Klausberger and Somogyi, 2008; Josselyn and Frankland, 2018; Pignatelli et al., 2019). Therefore, basic statistical data on the human hippocampal interneurons are necessary and are highly valuable for building models of this network.

This is particularly important for a better understanding of neurological and psychiatric disorders associated with different subpopulations of hippocampal neurons in Alzheimer's disease, major depressive disorder, schizophrenia or temporal lobe epilepsy. In certain neurological and psychiatric disorders, changes in the number, distribution, or connectivity of specific interneuronal subgroups expressing different markers in the hippocampus have been described (Maglóczky et al., 2000; Pelkey et al., 2017; Ruden et al., 2021). For example, the density of PV-positive hippocampal interneurons is reduced in patients with schizophrenia (Zhang and Reynolds, 2002), which may play an important role in the deficits observed in gamma oscillations (Lisman et al., 2008; Marín, 2012). The density of CR-expressing interneurons is reduced in epileptic patients, potentially leading to reduced local control over

hippocampal interneurons (Maglóczky et al., 2000; Tóth et al., 2010). According to animal models, malfunctioning of SOM-positive interneurons can also contribute to the network alterations occurring in epilepsy (Cossart et al., 2001; Drexel et al., 2022). Both SOM- and CR-positive interneurons have been shown to be vulnerable to ischemic injury (Johansen et al., 1987; Freund and Maglóczky, 1993), and some interneurons may also be differentially affected in Alzheimer's disease (Ramos et al., 2006; Palop and Mucke, 2016; Waller et al., 2020; Honoré et al., 2021). Therefore, understanding these pathomechanisms requires determining the number and distribution of interneuron types in the hippocampus of healthy subjects.

Here, we estimated the total number of PV-, SOM- and CR-positive inhibitory interneurons. We also estimated the total number of GABAergic terminals and synapses in different layers of the hippocampus and the proportion of synapses formed by PV-positive cells. Since the immunohistochemical detectability of certain proteins deteriorates rapidly with prolonged postmortem time (Wittner et al., 2005; Tóth et al., 2010; Gonzalez-Riano et al., 2017), a major advantage of this investigation was that we used fixative-perfused human brains with a short postmortem delay (less than 3.5 hours).

RESULTS

Volume of subregions and layers in one hippocampal hemisphere

In this study, we examined one hippocampal hemisphere from three human subjects with no known brain-related pathology (SKO24, SKO25, and SKO27). All hippocampi were sliced into blocks along the longitudinal axis. The volume of each hippocampal layer in each subregion (15 different areas) along the entire longitudinal extent of the hippocampus was precisely calculated in all subjects from neurolucida drawings of 7-10 PV-labeled representative sections from each tissue block (see Methods), distributed approximately evenly along the longitudinal axis of the fully sectioned hippocampi (see Methods, Figs. 1 and 2). Subfield boundaries [CA1-3 and dentate gyrus (DG)] were determined from adjacent calbindin-labeled sections (see Methods, Fig. 2C) using the following guidelines: calbindin-positive bundles of mossy fibers indicate the extent of the CA3 subfield, whereas pyramidal cells are densely calbindin-positive only in the CA2 region (Sloviter et al., 1991; Merino-Serrais et al., 2020). The border between CA1 and the prosubiculum is where the pyramidal cell layer suddenly fills almost the entire width of the layer between the str. moleculare and the alveus (Palomero-Gallagher et al., 2020).

We found large differences in the size of the hippocampi of the three subjects: the three investigated hippocampal hemispheres had volumes of 494 (SKO24), 717 (SKO25) and 1036 mm^3 (SKO27), i.e. the largest hippocampus was clearly more than twice as large as the smallest (Supplementary Tables). Different subregions contributed differently to the total volume (Supplementary Tables). CA1 was the largest in all subjects (50.1, 31.4, and 36.6% of the entire hippocampus in SKO24, SKO25, SKO27, respectively) followed by the CA3 (23.2, 30.9, and 28.3%) and dentate gyrus (17.4, 26.8, and 28.7%), which were about the same size. CA2 was the smallest in volume (9.3%, 10.9, and 6.4%). The contribution of each layer to a given subregion of the hippocampus was also calculated (see Supplementary Tables).

Estimation of the total number of different interneurons in the human hippocampus

To estimate the total number of specific interneurons, we used whole hippocampal sections immunostained for parvalbumin, somatostatin, or calretinin using ammonium nickel sulfate-intensified 3-3'-diaminobenzidine (DABNi) (Fig. 1-3, see Methods). Postmortem

delays of these subjects were short (2h 30 min- 3h 30 min) and the fixation of the tissue was optimal for all investigations (except SKO27 for SOM labeling, see below).

First, we measured the total volume of all 15 layers in each hippocampal section by investigating 7-10 complete hippocampal sections, either 60 or 100 µm thick, that were evenly distributed along the longitudinal axis of the hippocampus. Then, cell counting was performed on altogether 79 sections from all subjects for SOM, PV and CR. Immunolabeled cell bodies were quantified using the Neurolucida software following all stereological principles (see Methods, Fig. 2). Cell density values (number of cells/μm^3) were calculated for each layer of each hippocampal region (CA1-3, DG, Supplementary Tables). Total cell numbers of each layer were calculated separately for each subject by multiplying the cell densities with the respective volume values. It is known that different parts of the hippocampus along its longitudinal axis (head-body-tail in human hippocampus or ventral-dorsal hippocampus in rodents) have different afferent connections, perform different functions and therefore their interneuron composition may also differ (Strange et al., 2014). Therefore, in addition to the data for the entire hippocampus, we also provided cell density values separately for four/five consecutive blocks along the longitudinal axis of the hippocampus in the head-body-tail direction to represent potential differences (Supplementary Tables).

The total number of parvalbumin-positive interneurons in the human hippocampus

The distribution and morphology of parvalbumin-positive cells were similar in the three subjects (Fig.2 A, A', E, Fig. 3. A, B) and were consistent with some partial data reported earlier (Braak et al., 1991; Sloviter et al., 1991; Seress et al., 1993a; Wittner et al., 2001; Andrioli et al., 2007). Most of the parvalbumin-positive cells exhibited intense labeling and a large size with elongated dendrites (Fig. 3 A, B). Among the three investigated cell groups, the number of parvalbumin-positive cells was the lowest in the human hippocampus (n=45586 cells/ hemisphere, median). In the cornu ammonis, the majority (93%) of the cell bodies were in the str. pyramidale and oriens (Fig. 2 A', E). PV-positive cells were primarily found in the granule cell layer and in the hilus within the dentate gyrus (Fig. 2. E, Table 1, Supplementary Tables).

The total number of somatostatin-positive interneurons in the human hippocampus

Of the three cell markers, immunostaining against somatostatin neurons proved to be the most challenging, likely because of the lower expression levels of somatostatin, a neuropeptide, compared to the markers for the other two cell populations (which are calcium-binding molecules, parvalbumin and calretinin) and likely because somatostatin itself is mostly packed into large vesicles that are preferentially transported to different neuronal compartments Nevertheless, after fine-tuning the labelling protocols, labelling was reliable. DABNi-containing cells in the somatostatin-labeled sections were mildly labelled or dotty, and usually only their somata and parts of their proximal dendrites could be detected (Fig. 3 C, F). When analysing the results, we found that the SKO27 had far fewer cells than the other two subjects (Fig. 2 F) and these cells exhibited weaker labelling than cells in the other subjects. We therefore decided to exclude the data of SKO27 from the median calculation of total number of SOM-positive cells, nevertheless, we have also presented these slightly weaker results of this subject in Fig. 2 F in brackets.

The distribution of SOM-positive cells (Fig. 2 B, B', F) was consistent with some partial data reported in the literature (Chan-Palay, 1987). Briefly, the highest cell density (number of cells/ μm^3) was observed in the hilus and in CA3c str. pyramidale close to the hilus (Supplementary Tables, Fig 2 B, B', F, Fig. 3. C). Relatively high numbers of immunolabeled

cells were found in str. oriens of CA1-3 and in the CA1 str. pyramidale (Fig. 3D). Similar to parvalbumin-positive cells, almost no SOM-positive cells were found in the str. lacunosum-moleculare and radiatum in the cornu ammonis and in the str. moleculare of the dentate gyrus. The total number of somatostatin-positive cells in one hippocampal hemisphere was three times greater than that of parvalbumin-positive cells (n= 134 494, median, Table 1, Supp. Table 1).

The total number of calretinin-positive interneurons in the human hippocampus

It has been shown that the calretinin-positive cells are sensitive to ischaemic conditions (Freund and Maglóczky, 1993), and therefore their number rapidly decreases with the post-mortem delay (Tóth et al., 2010). Here, we used samples with short post-mortem delay. The quality of immunolabeling was uniformly high across the three subjects with most cells having strongly labelled cell bodies and dendritic trees (Fig. 3 E, F). The location and anatomical properties of immunolabeled cells were similar to those reported earlier (Seress et al., 1993b; Nitsch and Ohm, 1995). The individual cells displayed large morphological diversity, with most being relatively small, but some larger cells were also observed (Fig. 3.E, F). A high number of CR-positive cells was detected in all layers of the dentate gyrus (Fig. 2. C', G, Table 1, Supplementary Tables). The str. moleculare of the dentate gyrus contained numerous CR cell, but hardly any PV or SOM interneurons. CR cells were present in all layers of the cornu ammonis and were the most abundant out of the three interneuron types we investigated in the hippocampus. They were five times more numerous than PV-positive and 1.7 times more than SOM-positive neurons (n=227974, median, Fig. 1, Supplementary Tables).

The total number of GABAergic boutons in the human hippocampus

To model the network architecture of the human hippocampus, it is important to know the number of GABAergic boutons and their approximate number of synapses in different layers and subregions. We measured these data for all GABAergic boutons and parvalbumin-positive axon terminals. Estimation of these number for SOM terminals is not possible because SOM is present only within a few dense core vesicles, resulting in staining only in specific regions of these boutons, where these vesicles are located. In addition, there was a significant variability in the quality of staining and the quantity of stained boutons in different subjects and even in different sections of the same subjects. In addition, quantification of CR-containing axonal terminals would not have been particularly useful for modelling purposes because there are a large number of excitatory (and possibly inhibitory) afferent CR-axons that originate from external sources (Amaral and Cowan, 1980; Maglóczky et al., 1994; Borhegyi and Leranth, 1997; Bokor et al., 2002; Urbán et al., 2002; Tóth et al., 2010).

The total number of vGAT-positive boutons and synapses in the human hippocampus

For the quantification of total GABAergic boutons, we used immunoperoxidase labelling for vesicular GABA transporter (vGAT, see Methods). DABNi-labeled vGAT-positive boutons were manually outlined and counted in 3-dimension using stereological rules in stacks of serial electron microscopic images (see Methods, Fig. 4. A, A'). We first examined the quality of vGAT immunolabeling at both light and electron microscopic levels in all subjects. We found the highest number of strongly labelled boutons in SKO24, the only sample which was fixed with glutaraldehyde-containing fixative. The ultrastructural preservation of tissue in SKO24 was also the best among the three subjects. We therefore used this subject for all electron microscopic examinations.

The density of GABAergic boutons (number/mm^3) was evaluated in about 2800 to 18400 μm^3 sampling volumes, per hippocampal layers, per sample. We found that it is variable among hippocampal layers and subregions ranging from the 6.46 * 10^7/mm^3 highest value in str. moleculare to the 8.55 * 10^6/mm^3 lowest value in str. oriens of CA1. A single bouton can form not only one but several synapses (Bourne and Harris, 2012; Takács et al., 2015; Rigby et al., 2023). Therefore, to estimate the average number of synapses/bouton we 3-dimensionally reconstructed vGAT-positive boutons (n=36 in dendritic layers of CA1 and n=23 in str. moleculare of dentate gyrus) and their synapses in electron microscopic stacks imaged at a resolution optimal for the detection of synaptic membranes (3nm/pixel, see Methods, Fig. 4 C-D). We found that most of the boutons in the human hippocampus formed only one synapse and only some of them had two synapses. The average synapse number/boutons were 1.08 in the cornu ammonis and 1.04 in the molecular layer of the dentate gyrus. The synapse number/bouton was multiplied with the bouton density and the volume of the given layer in one hemisphere to get the total number of GABAergic synapses in any given layer (Table 1). Comparison of the layers shows that the largest proportion of hippocampal GABAergic synapses is in the CA1 str. pyramidale (4.32*10^9; 23.8% of all), followed by the str. moleculare of the dentate gyrus (2.78*10^9, 15.3%), the CA3 str. pyramidale (2.73*10^9; 15%) and CA1 str. lacunosum-moleculare (2.66*10^9; 14.7%). The other layers contribute between 7.2% (CA1 str. rad.) and 0.3% (CA3 str. lacunosum-moleculare) of the total GABAergic synapse number.

The total number of parvalbumin-positive boutons and synapses in the human hippocampus

The axonal labelling was also the densest in SKO24 among the parvalbumin labelled sections of the investigated samples, therefore we used this subject for estimating the parvalbumin-positive bouton density in hippocampal layers. In the somatic layers the parvalbumin-labelling was too dense (Fig.3 A, B), therefore we evaluated these layers using electron microscopic stacks similarly to vGAT-labeled sections (Fig. 4. B, B'). In the dendritic layers however, the parvalbumin-positive fibers were so rare that their investigation solely using electron microscopy would not have been practical. Therefore, these layers were evaluated using light microscopic image stacks, which were created with the Neurolucida system using a 100x oil immersion objective.

The density of parvalbumin-positive boutons (number/μm^3) was the highest in CA1 str. pyramidale (1.64*10^7) followed by str. granulosum (8.62 * 10^6), CA2 str. pyramidale (5.37* 10^6) and CA3 str. pyramidale (4.75*10^6). Values measured in other layers were orders of magnitude lower (Table 2.). The number of synapses/ bouton value was measured similarly to that of vGAT-positive boutons. This was higher in the case of PV-positive boutons in the somatic layers than that of vGAT positive boutons of the dendritic layers. We found 1.20 synapses/ bouton in str. pyramidale (n=20) and 1.33 synapses/ bouton in str. granulosum (n=21). We calculated the number of synapses formed by parvalbumin positive boutons (Table 1) and found that parvalbumin-positive synapses account for a significant proportion of all GABAergic synapses in the somatic layers of the human hippocampus (CA1 str. pyramidale: 43.7%; CA2 str. pyramidale: 13.3%; CA3 str. pyramidale: 17.2%, str. granulosum: 30.5%).

DISCUSSION

Using unbiased stereological methods, we estimated the absolute numbers of three major interneuron populations, the PV-positive cells, the SOM-positive cells, and the CR-positive cells, in each of the 15 layers of different hippocampal subregions in one hippocampal hemisphere of three human subjects. We found that there are approximately 45,600 PV-positive, 134,500 SOM-positive, and 228,000 CR-positive interneurons (median of three subjects for PV- and CR-positive interneurons, median of two subjects for SOM-positive interneurons) in one hemisphere of the human hippocampus (including the cornu ammonis and the dentate gyrus). In addition, we estimated the total number of GABAergic synapses in each layer of all hippocampal subregions using electron microscopy, and we also determined how many of these synapses are formed by parvalbumin-positive cells. We estimate that there are at least $1.82 * 10^{10}$ GABAergic synapses in the entire hippocampus, of which about $2.78 * 10^{9}$ are PV-positive, representing about 15.3% of all GABAergic synapses.

The size of the hippocampus does not correlate with the number of its interneurons.

The hippocampal volumes of the three subjects showed considerable variation (494, 717 and 1036 mm^3), similar to previous observations (Harding et al., 1998; Adler et al., 2018; Palomero-Gallagher et al., 2020), with the largest hippocampus being 2.1 times larger than the smallest. Yet we found that the largest one had only 1.26 times more PV, 1.39 times more SOM and 1.3 times more CR-positive neurons than the smallest hippocampus had. Comparing the two smaller hippocampi, we found that SKO25 is 1.45 times larger than SKO24 but has 10% fewer PV cells. Given that the sections underwent identical treatment procedures, with only a minor difference in fixative composition (specifically, the fixative used for SKO24 contained 0.05% glutaraldehyde in addition to other components, whereas the fixative for the other two brains did not), and considering the comparably short postmortem delay, the difference in size cannot be due to different degrees of tissue shrinkage. Instead, it probably reflects individual heterogeneity. However, these data suggest that the number of interneurons is a more tightly and more independently regulated variable than the size of the tissue itself, which may reflect differences in glial cells, neuronal connections or the number of other neurons.

The ratio of the examined interneurons to the total neuron number

The three interneuron populations investigated in this study cover only a fraction of all hippocampal interneurons, because there are several other types that do not express any of the markers tested (e.g. calbindin-positive cells and CCK/CB_1 receptor-positive interneurons (Lotstra and Vanderhaeghen, 1987; Seress et al., 1993a; Ludányi et al., 2008)).

According to previous estimates and counts, the areas of the hippocampus that we have investigated (CA1, 2, 3 and the dentate gyrus) contain a total of 20.73-35.7 $*10^6$ neurons, of which 5.28-16$*10^6$ are estimated to be in the CA area (West and Gundersen, 1990; Harding et al., 1998; Gandolfi et al., 2023). Using total neuronal cell numbers estimated by Harding et al, only about 0.22% of all neurons are PV-positive, 0.65% are SOM-positive, and 1.1% are CR-positive interneurons. This would mean that these three populations together represent only 2% of the cells in the entire hippocampus. Based on the CA1 cell model of Gandolfi et al (2023) and our data, 3.4% of all neurons would be PV, SOM or CR-positive. This is a surprising result because the proportion of total interneurons in the total cell population is about 10% in rodents (Woodson et al., 1989; Aika et al., 1994). In the rodent hippocampus, it is estimated that 23.9% of interneurons are parvalbumin-positive, 9.3% express somatostatin, and 19.4% are interneuron-specific cells, many of which contain calretinin (Bezaire and Soltesz, 2013). These

suggest that these three cell populations account for approximately half of all interneurons in rodents (i.e. 5% of the all neurons). It should be noted, however, that not all studies use the same rules to define the boundary between CA1 and the subiculum. Since the relative proportions of cells examined also differ between humans and rodents (see below), it is clear that it is not possible to extrapolate directly from rodent data to the human hippocampus.

Higher proportion of calretinin-containing interneurons in the human hippocampus compared to other interneurons

We found that the ratio of the three investigated cell groups in the human hippocampus is 1:3:5 (PV:SOM:CR), whereas in rodents this ratio is 2.6:1: 1.5 (Bezaire and Soltesz, 2013), i.e. while in rodents the parvalbumin-positive cells are the most numerous group, in the human hippocampus the calretinin-positive cells are five times more numerous. Single-cell RNA sequencing analysis has also revealed an evolutionary change in the proportion of inhibitory neuron classes with an increase of caudal ganglionic eminence-derived interneurons (including calretinin-positive interneurons) in the human neocortex (Hodge et al., 2019), confirming previous findings on progenitor cell migration (Hansen et al., 2013).

The number of calretinin-positive interneurons is particularly important because of their distinctive function among interneurons. Unlike other interneuron types, these cells are specialized to control other GABAergic cells in rodents (Gulyás et al., 1996). Similarly, in the human hippocampus, most of the postsynaptic target cells of bipolar calretinin-positive interneurons are calretinin-positive or other types of interneurons (Urbán et al., 2002; Tóth et al., 2010), although some of them innervate pyramidal cells as well. However, a considerable amount of human hippocampal calretinin-positive cell types are not present in rodent hippocampus and have unknown targets, like the multipolar cells at the border of stratum lacunosum-moleculare in CA1 or large neurons in the hilus (Urbán et al., 2002; Tóth et al., 2010). An increase in their number is consistent with a study that used connectomic screening of 3D-EM data across species and found an order of magnitude increase in the interneuron-to-interneuron network from mouse to human (Loomba et al., 2022).

Total number of GABAergic synapses and high proportion of parvalbumin-positive synapses in somatic layers

The density of vGAT-positive synapses in CA1, along with their differences between layers (specifically, being higher in str. pyramidale and lacunosum-moleculare compared to other layers), closely resembled the findings described by Montero-Crespo for symmetric synapses in CA1 (Montero-Crespo et al., 2020). We measured the density of synapses formed by vGAT-positive and PV-positive boutons in each layer throughout the entire cornu ammonis and dentate gyrus, allowing the calculation of the total number of boutons for each layer of all subregions of the hippocampus. We found that a significant proportion of these synapses in the somatic layers were established by parvalbumin-positive cells (13.3-43.7% in the cornu ammonis, 30.5% in the gyrus dentatus). These may be formed by local interneurons and extra-hippocampal afferents, but if most of these are established by local PV neurons then it suggests that a single PV cell may have the capacity to form a very large number of axon terminals.

METHODS

Human samples

Human hippocampus samples were obtained from three subjects who died due to causes not directly involving any brain disease or damage, and without having a medical history of neurological or psychiatric disorder. All procedures were carried out in compliance with the Declaration of Helsinki and approved by the Regional Committee of Science and Research Ethics of the Scientific Council of Health (ETT TUKEB 31443/2011/EKU, renewed: BM/15092-1/2023). The subjects went through an autopsy in the Department of Pathology of St. Borbála Hospital, Tatabánya, Hungary. Informed consent by relatives was obtained for the use of brain tissue and access to medical records for research purposes. Samples from the following subjects were used in the present study: SKO24: 79 years old, male, post-mortem interval (PMI): 2h 30 min, left hemisphere; SKO25: 87 years old, female, PMI: 3h 30 min, right hemisphere; SKO27: 76 years old, female, PMI: 3h 15 min, left hemisphere. Brains were removed after death and the internal carotid and vertebrate arteries were cannulated. First, physiological saline containing 0.33% heparin was perfused through this system (1.5 l in 30 min), after which perfusion continued with Zamboni fixative solution containing 4% paraformaldehyde, 0.2% picric acid and 0.05% (SKO24) or no glutaraldehyde (SKO25, SKO27) in 0.1 M phosphate buffer (PB, pH = 7.4, 2 h, 4 l). PMI was determined between the time of death and the start of perfusion by Zamboni fixative.

Sectioning

The whole hippocampi were dissected from the brains and cut into four (SKO24) or five (SKO25, 27) blocks perpendicular to their long axis (Fig. 1). To correctly identify all hippocampal subregions and layers, we followed the curvature of the hippocampus with the cuts. Therefore, in SKO25 and 27 each block ended in a so-called 'wedge part', the volumes of which layers were determined separately. In SKO24 only one large, triangular-shaped wedge block was cut, and the remaining blocks had parallel upper and lower cutting surfaces.

Blocks were embedded into 3% agarose and sections were cut on a Leica VT1200S vibratome. From all blocks, at least one but mostly more (2-3) sampling areas (located 1.5-3 mm away from each other) were sectioned at 60 or 100 µm. Sections in these sampling areas were collected in stereological order. All hippocampal blocks were completely sectioned, sections were collected and the data of sectioning was accurately recorded. Sections were rinsed in PB, cryoprotected in 30% sucrose in PB overnight, frozen over liquid nitrogen, and stored at -70 C until further processing.

Pre-embedding immunolabeling

From all sampling areas four neighboring sections were immunostained for parvalbumin, calretinin, somatostatin, and calbindin, respectively. For electron microscopic measurements selected sections were immunostained for vesicular GABA transporter (vGAT) or for PV. Sections were freeze-thawed twice over liquid nitrogen in 30% sucrose dissolved in PB. Then sections were washed in PB (2x10 min) and treated with 1% sodium borohydride in PB for 10 min. After extensive washes in PB (5x5min) endogenous peroxidase-like activity was blocked by 1% hydrogen peroxide in TBS for 10 min. Then sections were transferred into 0.05 M Tris-buffered saline (pH 7.4; TBS) and blocked in 2% bovine serum albumin (Sigma-Aldrich) and 0.1 g/ml lysine and glycine in TBS. Then, sections were incubated in a solution of mouse anti-parvalbumin (1:5000, Swant, Cat. No. 235)/ guinea pig anti-somatostatin (1:1000, Synaptic Systems, Cat. No. 366 004), mouse anti-calretinin (1:5000, Swant, Cat. No. 6B3) rabbit anti-calbindin (1:10 000, gift from Prof. Kenneth Baimbridge, code: 8702) or goat anti-vGAT [1:1000, gift from Prof. Masahiko Watanabe (Iwakura et al., 2012; Kudo et al.,

2012)] primary antibodies diluted in TBS containing 0.05% sodium azide for 2 days. After repeated washes in TBS, the sections were incubated in goat anti-mouse (Cat. No. BA-2000)/ goat anti-guinea pig (BA-7000)/ goat anti-rabbit (BA-1000) or horse anti-goat (BA-9500) biotinylated secondary antibodies overnight (1:500, Vector Laboratories) followed by extensive washes in TBS (3x10 min) and in VECTASTAIN® Elite® avidin–biotinylated horseradish peroxidase complex (Standard) for 1.5 h (1:250 in TBS; Vector Laboratories).

The immunoperoxidase reaction was developed using ammonium nickel sulfate-intensified 3-3'-diaminobenzidine (DABNi) as the chromogen. Antibodies used in this study were tested for specificity. No specific-like staining was observed without primary antibodies. After washes in PB, sections were contrasted with 0.25% (for cell counting in the light microscope) or 0.5% (for electron microscopic investigations) osmium-tetroxide in PB on ice for 15 min. The sections were then dehydrated in ascending alcohol series and in acetonitrile and embedded in Durcupan (ACM; Fluka). During dehydration, the sections for electron microscopic investigations were treated with 1% uranyl acetate in 70% ethanol for 30 min.

Cell counting in the light microscope

For each of the three interneuron-populations, 7-10 hippocampal sections (8.8 ±1.1) at approximately equal distances from each other and in precisely known locations along the longitudinal axis of the hippocampus have been processed in each subject. Hippocampal layers of PV, SOM and CR-labeled sections were outlined using the Neurolucida software attached to a Zeiss Axioscope2 microscope with a 5× objective (MBF Bioscience). Boundaries of hippocampal subregions (CA1, 2, 3, DG) in each section were defined using the neighboring calbindin labelled sections by applying the following rules: calbindin-positive bundles of mossy fibers indicate the extent of the CA3 subregion, whereas pyramidal cells are densely calbindin-positive only in the CA2 region (Sloviter et al., 1991; Merino-Serrais et al., 2020). The pyramidal cell layer expands and occupies almost all space between the alveus and dentate gyrus in the subiculum which does not apply to CA1 (Palomero-Gallagher et al., 2020). PV, SOM, or CR-positive cell bodies in CA1-3 and the dentate gyrus were marked on the drawings using the Neurolucida software with a 40x oil-immersion objective. In human samples, OsO_4-treatment caused brown background-like labeling of cell bodies that is likely caused by the osmification of lipofuscin. This was clearly distinguishable from the specific DABNi-labeling of interneurons, which was black and labeled the dendrites of the cells as well in addition to their somata (see Fig. 3). All cells were considered positive (even those that were faintly labeled or dotty) if they were black and had at least one dendrite. According to stereological principles, cell bodies were only marked on drawings and counted if they did not intersect the bottom of the section, but were counted if cut on the surface. In each sampled section, for each layer of each subregion (CA1, 2, 3: str. oriens, pyramidale, radiatum and lacunosum-moleculare, dentate gyrus: hilus, str. granulosum, and moleculare) a density value was calculated by dividing the cell count obtained by the area of the sampled part of the given section. To obtain the total cell count of a block of the human hippocampus, the densities of the two bounding sampled sections (60 or 100 μm) were averaged and multiplied by the volume of the respective layer in the block. Finally, the cell counts estimated in these blocks were summed to give the total hippocampal cell count in every layer (in every subregion) of the hippocampus. Because we utilized the same sections for both total volume- and cell density measurements, we did not apply adjustments for tissue shrinkage/dilatation.

Measurement of the volume of hippocampal layers

Neurolucida drawings of PV-labeled sections (n=7-10 sections/subjects) in precisely known locations along the long axis of the hippocampus were used for volume measurements (see above). Subregions (CA1-3, DG) in these sections were defined also with the help of the

neighboring calbindin-labeled sections (see above). The areas of each hippocampal layer in each subregion (CA1, 2, 3: str. oriens, pyramidale, radiatum and lacunosum-moleculare, dentate gyrus: hilus, str. granulosum, and moleculare), were measured using the Adobe Photoshop software. The volume of each hippocampal layer in each subregion was defined for all tissue blocks. In the "wedge" parts (with precisely known locations along the longitudinal axis of the hippocampus), sections were labeled for calbindin. The area of hippocampal subregions in each of these sections was defined using the Cavalieri Estimator probe in StereoInvestigator (MBF Bioscience). The volumes of each layer of each block were summed to give the total volume of the given layer in the hippocampal hemisphere.

Sample preparation for scanning electron microscopy (SEM)

The tissue was cut out and mounted on the top of resin blocks with cyanoacrylate glue, then ultrathin (70 nm thick) sections were cut with a diamond knife (Diatome, Biel, Switzerland) mounted on an ultramicrotome (EM UC6, Leica, Wetzlar, Germany). Ribbons of consecutive ultrathin sections (n= 55-200 sections/sample) were transferred to silicon wafers (a special conductive section carrier, Ted Pella).

SEM imaging

Because of the very dense DABNi-labelling, the number of DABNi-labeled boutons could not be accurately determined at the light microscopic level in the vGAT-labeled sections and in the somatic layers of the PV-labeled sections. Therefore, we used an electron microscope to obtain these values. The sections were imaged with scanning electron microscopy (SEM, FEI Apreo, Eindhoven, The Netherlands) in backscattered mode. We used a FEI Apreo field emission gun (FEG) SEM (Thermo Scientific) and a T1 in-column detector to record the backscattered electrons. The micrographs were acquired with an array tomography plugin in MAPs software (version: 3.17, https://www.thermofisher.com/hu/en/home/electron-microscopy/products/software-em-3d-vis/maps-software.html), which can facilitate the automatic acquisition of SEM images. The following imaging parameters were used: 4 mm working distance at a high vacuum with 0.1 nA beam current, 2 kV high voltage, 3 µs/pixel dwell time and 9 nm pixel size for bouton density measurements and 6 µs/pixel dwell time and 3 nm pixel size for analysis of number of synapses/bouton. The micrographs were 6000x6000 (bouton density measurements, see below) or 8000x8000 pixels (analysis of number of synapses/bouton, see below) and we recorded 45-127 sections with 70 nm thickness.

Correction for EM section compression during diamond knife sectioning

The force applied by the diamond knife during the cutting of serial EM sections compresses the sections. The correction factor for section compression was calculated by dividing the width of the tissue block face in the resin with the width of EM sections measured perpendicular to the diamond knife blade (Y plane). The measurements were performed using Zeiss Axioplan2 light microscope. The correction factor in the Y plane was 1.27 ± 0.05 (mean ± SD, n= 15 blocks). There was no change in the EM section dimension in the direction parallel (X plane) with the diamond knife edge. The area of sampled ROI was calculated by multiplying the X length and the corrected Y lengths of the ROI. It was multiplied by the number of sections and section thickness for the calculation of the volume of sampled tissue.

SEM Image analysis

After SEM image series were collected, image post-processing was done in Fiji ImageJ (Schindelin et al., 2012). The SEM stacks were imported into Fiji TrakEM2 plugin15 and finely aligned. The boutons and synapses were segmented using the IMOD (version 4.9,

https://bio3d.colorado.edu/imod) package (Kremer et al., 1996) in which the delineation was performed on a Wacom Cintiq 27QHD Creative Pen and display tablet.

Bouton density measurements

Randomly selected sampling areas were imaged in every section of a series of 70 nm-thick ultrathin sections (n= 53-127 serial sections) using a scanning electron microscope (see above). The micrographs were 6000x6000 pixels with 9 nm pixel size. After fine alignment of the image series (see above), boutons were manually labeled using IMOD software (see above) in the images throughout the series and quantified in 3D using stereological rules. We used the physical disector principle. Counting was done within a stereological counting frame and boutons were only counted if they were not present in the last section. The sampling volume was 2800- 19800 μm^3 / hippocampal layers/ sample. In layers where the density of PV-labeled boutons was very low (i.e., dendritic layers), we counted the boutons at light microscopic level using stacks of images created with the Neurolucida system attached to a Zeiss Axioscope2 microscope with a 100× immersion oil objective (MBF Bioscience). The sampling volume in the light microscope was 598 000-627 000 μm^3 / hippocampal layers/ sample.

Determination of synapse number/ bouton

Randomly selected sampling areas were imaged in every section of a series of 70 nm-thick ultrathin sections (n=45-67 serial sections) using a scanning electron microscope at 3 nm/pixel resolution (see above). DABNi-labeled boutons and their synapses were reconstructed only if they were fully included in the series and the preservation of surrounding tissue was sufficient to identify synapses. Parallel appositions between the membranes of the presynaptic bouton and the putative postsynaptic target were regarded as synapses if they displayed a widening of the extracellular space at the presumptive synaptic cleft and a postsynaptic membrane thickening. Synapse number/ boutons measurements were done in vGAT-labeled sections in the case of dendritic layers and PV-labeled sections in the case of somatic layers.

REFERENCES

Adler DH et al. (2018) Characterizing the human hippocampus in aging and Alzheimer's disease using a computational atlas derived from ex vivo MRI and histology. Proc Natl Acad Sci U S A 115:4252–4257.

Aika Y, Ren JQ, Kosaka K, Kosaka T (1994) Quantitative analysis of GABA-like-immunoreactive and parvalbumin-containing neurons in the CA1 region of the rat hippocampus using a stereological method, the disector. Exp brain Res 99:267–276.

Amaral DG, Cowan WM (1980) Subcortical afferents to the hippocampal formation in the monkey. J Comp Neurol 189:573–591.

Andrioli A, Alonso-Nanclares L, Arellano JI, DeFelipe J (2007) Quantitative analysis of parvalbumin-immunoreactive cells in the human epileptic hippocampus. Neuroscience 149:131–143.

Bezaire MJ, Soltesz I (2013) Quantitative assessment of CA1 local circuits: knowledge base for interneuron-pyramidal cell connectivity. Hippocampus 23:751–785.

Bokor H, Csáki Á, Kocsis K, Kiss J (2002) Cellular architecture of the nucleus reuniens thalami and its putative aspartatergic/glutamatergic projection to the hippocampus and medial septum in the rat. Eur J Neurosci 16:1227–1239.

Borhegyi Z, Leranth C (1997) Distinct substance P- and calretinin-containing projections from the supramammillary area to the hippocampus in rats; a species difference between rats and monkeys. Exp brain Res 115:369–374.

Bourne JN, Harris KM (2012) Nanoscale analysis of structural synaptic plasticity. Curr Opin Neurobiol 22:372–382.

Braak E, Strotkamp B, Braak H (1991) Parvalbumin-immunoreactive structures in the hippocampus of the human adult. Cell Tissue Res 264:33–48.

Brunton BW, Beyeler M (2019) Data-driven models in human neuroscience and neuroengineering. Curr Opin Neurobiol 58:21–29.

Cai DJ et al. (2016) A shared neural ensemble links distinct contextual memories encoded close in time. Nature 534:115–118.

Chan-Palay V (1987) Somatostatin immunoreactive neurons in the human hippocampus and cortex shown by immunogold/silver intensification on vibratome sections: coexistence with neuropeptide Y neurons, and effects in Alzheimer-type dementia. J Comp Neurol 260:201–223.

Cossart R, Dinocourt C, Hirsch JC, Merchan-Perez A, De Felipe J, Ben-Ari Y, Esclapez M, Bernard C (2001) Dendritic but not somatic GABAergic inhibition is decreased in experimental epilepsy. Nat Neurosci 4:52–62.

DeFelipe J et al. (2013) New insights into the classification and nomenclature of cortical GABAergic interneurons. Nat Rev Neurosci 14:202–216.

DeFelipe J, Hendry SH, Jones EG (1989) Visualization of chandelier cell axons by parvalbumin immunoreactivity in monkey cerebral cortex. Proc Natl Acad Sci U S A 86:2093–2097.

Drexel M, Rahimi S, Sperk G (2022) Silencing of Hippocampal Somatostatin Interneurons Induces Recurrent Spontaneous Limbic Seizures in Mice. Neuroscience 487:155–165.

Freund TF, Buzsáki G (1996) Interneurons of the hippocampus. Hippocampus 6:347–470.

Freund TF, Maglóczky Z (1993) Early degeneration of calretinin-containing neurons in the rat hippocampus after ischemia. Neuroscience 56:581–596.

Gandolfi D, Mapelli J, Solinas SMG, Triebkorn P, D'Angelo E, Jirsa V, Migliore M (2023) Full-scale scaffold model of the human hippocampus CA1 area. Nat Comput Sci 3:264–276.

Gonzalez-Riano C, Tapia-González S, García A, Muñoz A, DeFelipe J, Barbas C (2017)

Metabolomics and neuroanatomical evaluation of post-mortem changes in the hippocampus. Brain Struct Funct 222:2831–2853.
Goode TD, Tanaka KZ, Sahay A, McHugh TJ (2020) An Integrated Index: Engrams, Place Cells, and Hippocampal Memory. Neuron 107:805–820.
Gulyás AI, Hájos N, Freund TF (1996) Interneurons containing calretinin are specialized to control other interneurons in the rat hippocampus. J Neurosci 16:3397–3411.
Hansen D V, Lui JH, Flandin P, Yoshikawa K, Rubenstein JL, Alvarez-Buylla A, Kriegstein AR (2013) Non-epithelial stem cells and cortical interneuron production in the human ganglionic eminences. Nat Neurosci 16:1576–1587.
Harding AJ, Halliday GM, Kril JJ (1998) Variation in hippocampal neuron number with age and brain volume. Cereb Cortex 8:710–718.
Hodge RD et al. (2019) Conserved cell types with divergent features in human versus mouse cortex. Nature 573:61–68.
Honoré E, Khlaifia A, Bosson A, Lacaille JC (2021) Hippocampal Somatostatin Interneurons, Long-Term Synaptic Plasticity and Memory. Front Neural Circuits 15:1–24.
Iwakura a., Uchigashima M, Miyazaki T, Yamasaki M, Watanabe M (2012) Lack of Molecular-Anatomical Evidence for GABAergic Influence on Axon Initial Segment of Cerebellar Purkinje Cells by the Pinceau Formation. J Neurosci 32:9438–9448.
Johansen FF, Zimmer J, Diemer NH (1987) Early loss of somatostatin neurons in dentate hilus after cerebral ischemia in the rat precedes CA-1 pyramidal cell loss. Acta Neuropathol 73:110–114.
Josselyn SA, Frankland PW (2018) Memory Allocation: Mechanisms and Function. Annu Rev Neurosci 41:389–413.
Klausberger T (2009) GABAergic interneurons targeting dendrites of pyramidal cells in the CA1 area of the hippocampus. Eur J Neurosci 30:947–957.
Klausberger T, Somogyi P (2008) Neuronal diversity and temporal dynamics: the unity of hippocampal circuit operations. Science 321:53–57.
Kosaka T, Wu JY, Benoit R (1988) GABAergic neurons containing somatostatin-like immunoreactivity in the rat hippocampus and dentate gyrus. Exp brain Res 71:388–398.
Kremer JR, Mastronarde DN, McIntosh JRR (1996) Computer visualization of three-dimensional image data using IMOD. J Struct Biol 116:71–76 Available at: http://www.sciencedirect.com/science/article/pii/S1047847796900131%5Cnhttp://www.ncbi.nlm.nih.gov/pubmed/8742726.
Kudo T, Uchigashima M, Miyazaki T, Konno K, Yamasaki M, Yanagawa Y, Minami M, Watanabe M (2012) Three types of neurochemical projection from the bed nucleus of the stria terminalis to the ventral tegmental area in adult mice. J Neurosci Off J Soc Neurosci 32:18035–18046.
Lisman JE, Coyle JT, Green RW, Javitt DC, Benes FM, Heckers S, Grace A a. (2008) Circuit-based framework for understanding neurotransmitter and risk gene interactions in schizophrenia. Trends Neurosci 31:234–242.
Loomba S, Straehle J, Gangadharan V, Heike N, Khalifa A, Motta A, Ju N, Sievers M, Gempt J, Meyer HS, Helmstaedter M (2022) Connectomic comparison of mouse and human cortex. Science 377:eabo0924.
Lotstra F, Vanderhaeghen JJ (1987) Distribution of immunoreactive cholecystokinin in the human hippocampus. Peptides 8:911–920.
Ludányi A, Eross L, Czirják S, Vajda J, Halász P, Watanabe M, Palkovits M, Maglóczky Z, Freund TF, Katona I (2008) Downregulation of the CB1 cannabinoid receptor and related molecular elements of the endocannabinoid system in epileptic human hippocampus. J Neurosci Off J Soc Neurosci 28:2976–2990.

Maglóczky Z, Acsády L, Freund TF (1994) Principal cells are the postsynaptic targets of supramammillary afferents in the hippocampus of the rat. Hippocampus 4:322–334.
Maglóczky Z, Wittner L, Borhegyi Z, Halász P, Vajda J, Czirják S, Freund TF (2000) Changes in the distribution and connectivity of interneurons in the epileptic human dentate gyrus. Neuroscience 96:7–25.
Marín O (2012) Interneuron dysfunction in psychiatric disorders. Nat Rev Neurosci 13:107–120.
Merino-Serrais P, Tapia-González S, DeFelipe J (2020) Calbindin immunostaining in the CA1 hippocampal pyramidal cell layer of the human and mouse: A comparative study. J Chem Neuroanat 104:101745.
Montero-Crespo M, Dominguez-Alvaro M, Rondon-Carrillo P, Alonso-Nanclares L, DeFelipe J, Blazquez-Llorca L (2020) Three-dimensional synaptic organization of the human hippocampal CA1 field. Elife 9.
Nitsch R, Ohm TG (1995) Calretinin immunoreactive structures in the human hippocampal formation. J Comp Neurol 360:475–487.
Palomero-Gallagher N, Kedo O, Mohlberg H, Zilles K, Amunts K (2020) Multimodal mapping and analysis of the cyto- and receptorarchitecture of the human hippocampus. Brain Struct Funct 225:881–907.
Palop JJ, Mucke L (2016) Network abnormalities and interneuron dysfunction in Alzheimer disease. Nat Rev Neurosci 17:777–792.
Pelkey KA, Chittajallu R, Craig MT, Tricoire L, Wester JC, McBain CJ (2017) Hippocampal gabaergic inhibitory interneurons. Physiol Rev 97:1619–1747.
Pignatelli M, Ryan TJ, Roy DS, Lovett C, Smith LM, Muralidhar S, Tonegawa S (2019) Engram Cell Excitability State Determines the Efficacy of Memory Retrieval. Neuron 101:274–284.
Ramos B, Baglietto-Vargas D, Rio JC del, Moreno-Gonzalez I, Santa-Maria C, Jimenez S, Caballero C, Lopez-Tellez JF, Khan ZU, Ruano D, Gutierrez A, Vitorica J (2006) Early neuropathology of somatostatin/NPY GABAergic cells in the hippocampus of a PS1 × APP transgenic model of Alzheimer's disease. Neurobiol Aging 27:1658–1672.
Rigby M, Grillo FW, Compans B, Neves G, Gallinaro J, Nashashibi S, Horton S, Pereira Machado PM, Carbajal MA, Vizcay-Barrena G, Levet F, Sibarita J-B, Kirkland A, Fleck RA, Clopath C, Burrone J (2023) Multi-synaptic boutons are a feature of CA1 hippocampal connections in the stratum oriens. Cell Rep 42:112397.
Roy DS, Kitamura T, Okuyama T, Ogawa SK, Sun C, Obata Y, Yoshiki A, Tonegawa S (2017) Distinct neural circuits for the formation and retrieval of episodic memories. Cell 170:1000-1012.e19.
Ruden JB, Dugan LL, Konradi C (2021) Parvalbumin interneuron vulnerability and brain disorders. Neuropsychopharmacology 46:279–287.
Schindelin J, Arganda-Carreras I, Frise E, Kaynig V, Longair M, Pietzsch T, Preibisch S, Rueden C, Saalfeld S, Schmid B, Tinevez J-Y, White DJ, Hartenstein V, Eliceiri K, Tomancak P, Cardona A (2012) Fiji: an open-source platform for biological-image analysis. Nat Methods 9:676–682.
Seress L, Gulyás AI, Ferrer I, Tunon T, Soriano E, Freund TF (1993a) Distribution, morphological features, and synaptic connections of parvalbumin- and calbindin D28k-immunoreactive neurons in the human hippocampal formation. J Comp Neurol 337:208–230.
Seress L, Nitsch R, Leranth C (1993b) Calretinin immunoreactivity in the monkey hippocampal formation--I. Light and electron microscopic characteristics and co-localization with other calcium-binding proteins. Neuroscience 55:775–796.
Sloviter RS, Sollas AL, Barbaro NM, Laxer KD (1991) Calcium-binding protein (calbindin-

D28K) and parvalbumin immunocytochemistry in the normal and epileptic human hippocampus. J Comp Neurol 308:381–396.
Somogyi P (1977) A specific “axo-axonal” interneuron in the visual cortex of the rat. Brain Res 136:345–350.
Somogyi P, Freund TF, Cowey A (1982) The axo-axonic interneuron in the cerebral cortex of the rat, cat and monkey. Neuroscience 7:2577–2607.
Strange BA, Witter MP, Lein ES, Moser EI (2014) Functional organization of the hippocampal longitudinal axis. Nat Rev Neurosci 15:655–669.
Szőnyi A, Sos K, Nyilas R, Schlingloff D, Domonkos A, Takács V, Pósfai B, Hegedüs P, Priestley J, Gundlach A, Gulyás AI, Varga V, Losonczy A, Freund TF, Nyiri G (2019) Brainstem nucleus incertus controls contextual memory formation. Science 364.
Takács VT, Szőnyi A, Freund TF, Nyiri G, Gulyás AI (2015) Quantitative ultrastructural analysis of basket and axo-axonic cell terminals in the mouse hippocampus. Brain Struct & Funct 220:919–940.
Tóth K, Ero’ss L, Vajda J, Halász P, Freund TF, Maglóczky Z (2010) Loss and reorganization of calretinin-containing interneurons in the epileptic human hippocampus. Brain 133:2763–2777.
Urbán Z, Maglóczky Z, Freund TF (2002) Calretinin-containing interneurons innervate both principal cells and interneurons in the CA1 region of the human hippocampus. Acta Biol Hung 53:205–220.
Waller R, Mandeya M, Viney E, Simpson JE, Wharton SB (2020) Histological characterization of interneurons in Alzheimer’s disease reveals a loss of somatostatin interneurons in the temporal cortex. Neuropathology 40:336–346.
West MJ, Gundersen HJ (1990) Unbiased stereological estimation of the number of neurons in the human hippocampus. J Comp Neurol 296:1–22.
Wittner L, Eross L, Czirják S, Halász P, Freund TF, Maglóczky Z (2005) Surviving CA1 pyramidal cells receive intact perisomatic inhibitory input in the human epileptic hippocampus. Brain 128:138–152.
Wittner L, Maglóczky Z, Borhegyi Z, Halász P, Tóth S, Eross L, Szabó Z, Freund TF (2001) Preservation of perisomatic inhibitory input of granule cells in the epileptic human dentate gyrus. Neuroscience 108:587–600.
Woodson W, Nitecka L, Ben-Ari Y (1989) Organization of the GABAergic system in the rat hippocampal formation: A quantitative immunocytochemical study. J Comp Neurol 280:254–271.
Zhang ZJ, Reynolds GP (2002) A selective decrease in the relative density of parvalbumin-immunoreactive neurons in the hippocampus in schizophrenia. Schizophr Res 55:1–10.
Zichó K, Sos KE, Papp P, Barth AM, Misák E, Orosz Á, Mayer MI, Sebestény RZ, Nyiri G (2023) Fear memory recall involves hippocampal somatostatin interneurons. PLoS Biol.

ACKNOWLEDGEMENTS

We thank E. Szépné Simon, N. Kriczky, and Z. Hajós for helping with the experiments, Q. Nguyen for helping with Neurolucida drawings and G. Goda and K. Iványi for other assistance. We thank the Department of Pathology, Saint Borbála Hospital, Tatabánya, Hungary and the Human Brain Research Laboratory at the Institute of Experimental Medicine (IEM) for providing human brain tissue. We thank the Electron Microscopy Center at the IEM for technical help with the FEI Apreo scanning electron microscope and the Hitachi H-7100 transmission electron microscope and S. Kőszegi for help in image acquisition. We acknowledge the Light Microscopy Center at the IEM for the use of the PANNORAMIC MIDI II digital slide scanner and thank P. Vági and L. Barna for their assistance in image acquisition.

FUNDING

This work was supported by the Frontline Research Excellence Program of the Hungarian National Research, Development and Innovation Office (NRDI Fund 133837), the Hungarian Brain Research Program NAP3.0 (NAP2022-I-1/2022), the European Union project RRF-2.3.1-21-2022-00004 within the framework of the Artificial Intelligence National Laboratory and the European Union project RRF-2.3.1-21-2022-00011 within the framework of the Translational Neuroscience National Laboratory to G.N.; the Hungarian Brain Research Program NAP2.0 (2017-1.2.1-NKP-2017-00002) to Z.M., T.F.F. and G.N.; the European Union Human Brain Project (SGA3, 945539) to T.F.F. and G.N.; and the New National Excellence Program of the Ministry for Innovation and Technology and the Ministry of Human Capacities, ÚNKP-23-6-I to T.Z. and ÚNKP-23-3-I-SE-48 to Á.O.

FIGURES

Fig. 1. Sectioning procedure.

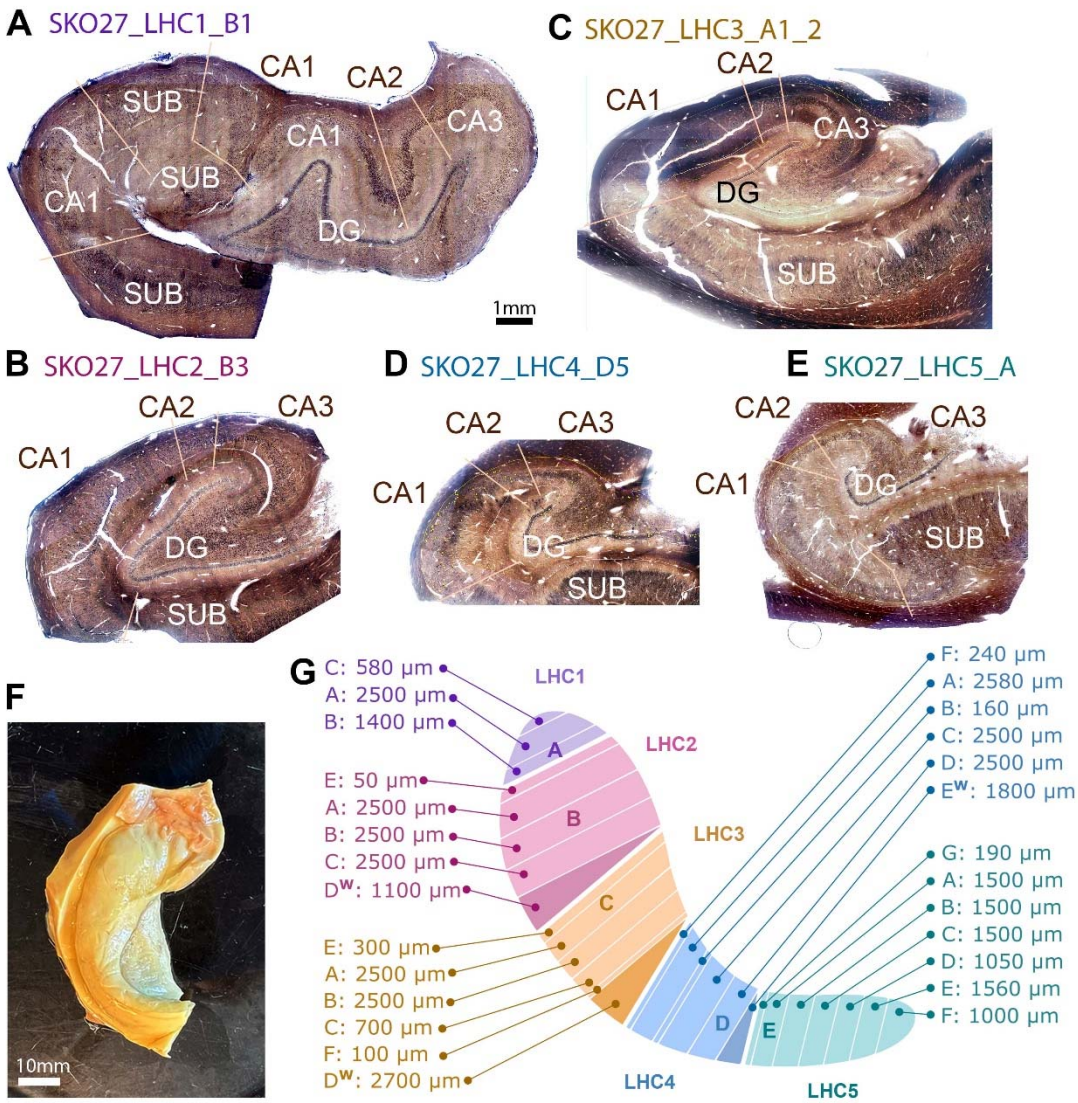

This illustration represents the sectioning procedure (SKO27 is shown here that was similar to the sectioning of the other two hippocampi). Whole hippocampal hemispheres were dissected from the brains (F) and cut into four or five blocks (left hippocampus 1-5 blocks: LHC1-5) perpendicular to their long axis (G). To correctly identify all hippocampal subregions and layers, the curvature of the hippocampus was followed by using 3 precisely reconstructed wedges (LHC2 D^W, LHC3 $D^{W,}$ and LHC4 E^W in G), the volumes of which layers were determined separately (see Methods). All blocks (LHC1-5) were embedded in agarose and completely sectioned while data of section numbers and thickness was accurately recorded for volume measurements (G). A-E: Light microscopic images of 100 µm-thick human hippocampal sections labeled for parvalbumin. The cutting positions of the sections in A-E are indicated in G with letters A-E. Sections from the sampling areas (n=10, for each immunolabeling, including sections in A-E) were used to estimate total interneuron numbers in the hippocampus. Some cracks caused by the flat embedding procedure were also reconstructed and taken into account for both volume and cell density estimation.

Fig. 2. Distribution and total numbers of different types of interneurons in the human hippocampus.

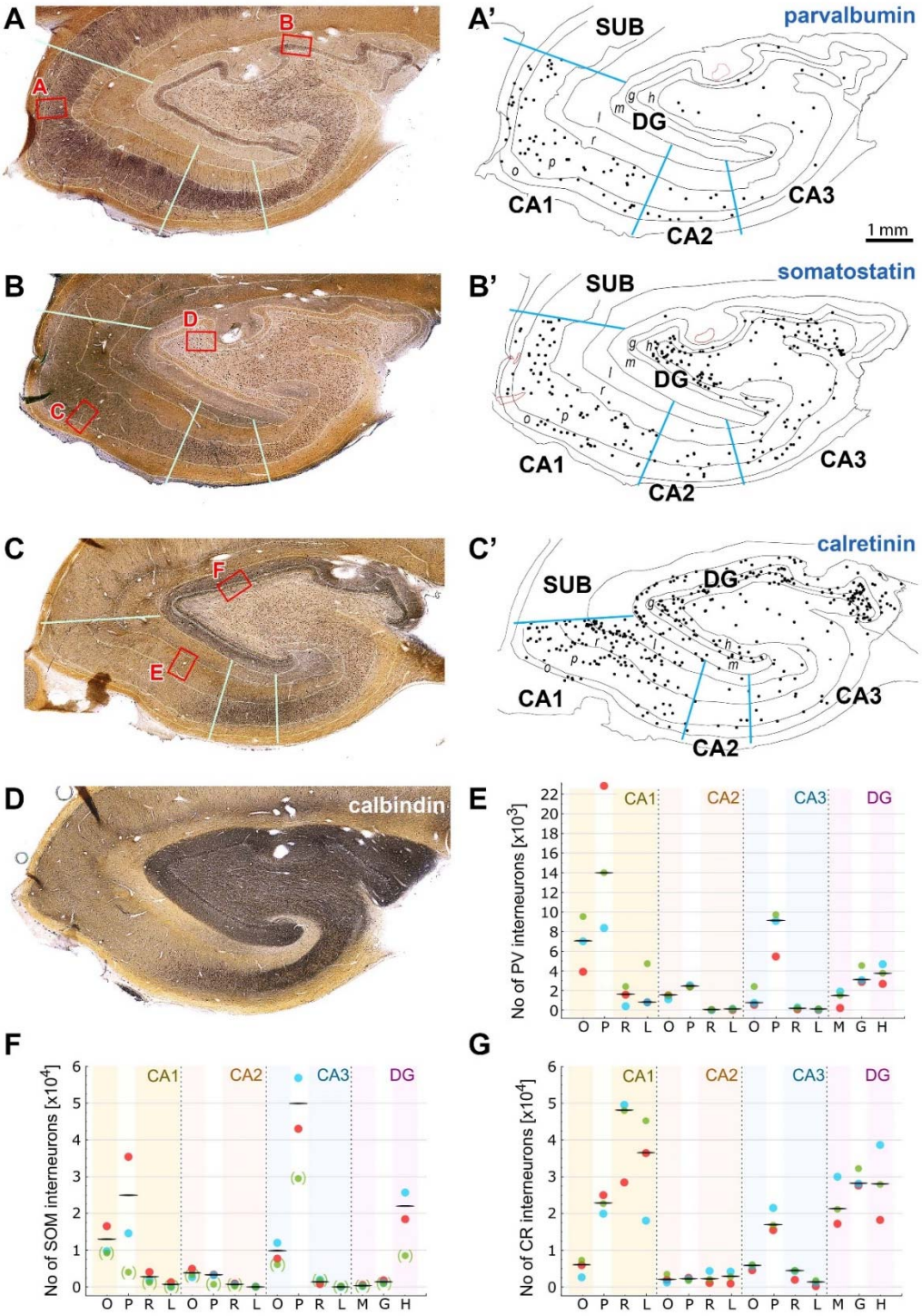

Hippocampal sections immunolabeled for PV (A), SOM (B), and CR (C) were used to estimate the total interneuron numbers in the hippocampus. Boundaries of hippocampal subregions in each section were defined using the neighboring calbindin labelled sections (D, see Methods). Four neighboring sections from the left hippocampal hemisphere of SKO24 are shown here to illustrate the characteristic differences in the distribution and density of the different interneurons. The areas highlighted with red are illustrated in Fig. 3 at higher

magnification. A’-C’: Neurolucida drawings of hippocampal sections A-C. DABNi-labeled cell bodies were counted using stereological rules (see Methods) and indicated in the drawings with black dots. Subregion boundaries are shown with blue lines. E-G: Total numbers of interneurons in hippocampal layers in one hemisphere. Different colors represent data from different subjects (red: SKO24 left-, blue: SKO25 right-, and green: SKO27 left hemisphere). Medians are shown with black lines. In SKO27, the somatostatin labeling was much weaker than in the other two hippocampi, therefore its data are shown in brackets and only data from the other two subjects were used for the median. DG: dentate gyrus, SUB: subiculum, o: stratum (str.) oriens; p: str. pyramidale, r: str. radiatum, l: str. lacunosum-moleculare, m: str. moleculare, g: str. granulosum, h: hilus.

Fig. 3. PV-, SOM- and CR-positive cells in the human hippocampus.

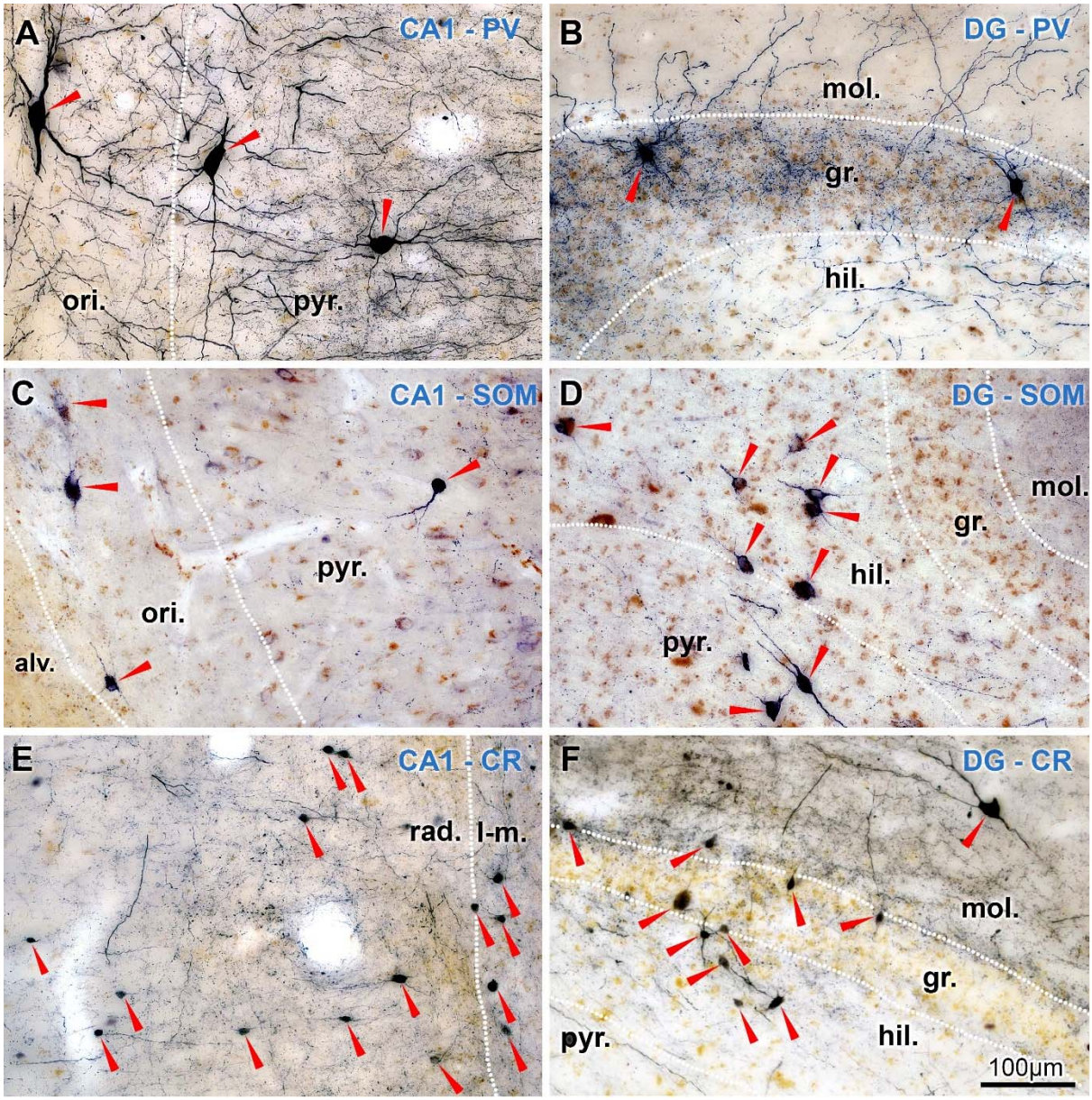

Areas highlighted with red rectangles in Fig. 2 are illustrated here. Cells were immunolabelled using ammonium nickel sulfate-intensified 3-3'-diaminobenzidine (DABNi) resulting in a bluish-black color, which could be easily distinguished from the light brown background color of cell bodies (see e.g. granule cell bodies in str. granulosum). Positive interneurons are indicated with red arrowheads. DG: dentate gyrus, ori.: statum (str.) oriens; pyr.: str. pyramidale, rad.: str. radiatum, l-m.: str. lacunosum-moleculare, mol.: str. moleculare, gr.: str. granulosum, hil.: hilus.

Fig. 4. Electron microscopic analysis of vesicular GABA-transporter (vGAT) and parvalbumin (PV) -positive boutons in the human hippocampus.

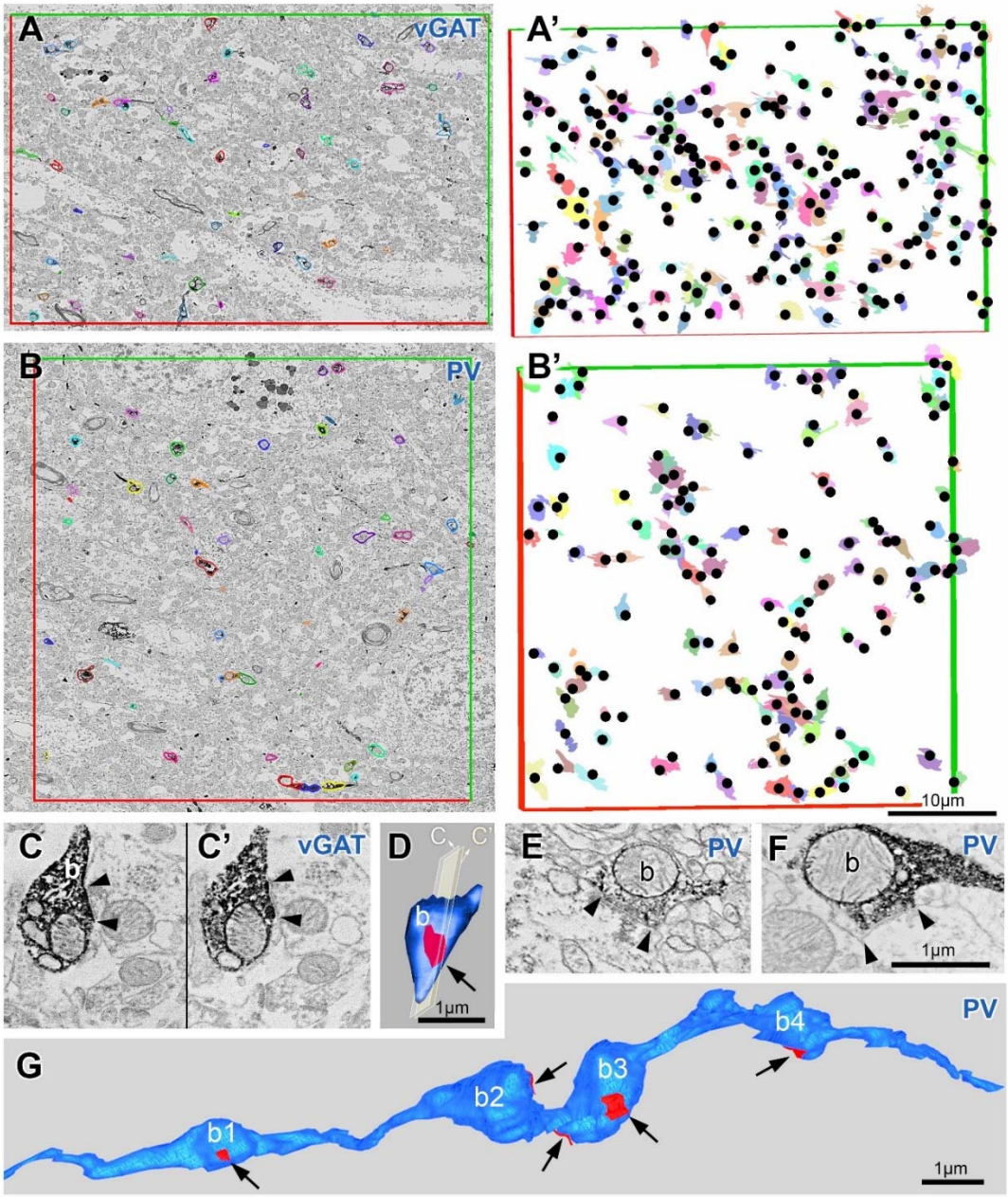

A, B: Electron micrographs of randomly selected areas from CA1 str. pyramidale immunolabelled for vGAT (A) or PV (B). These areas were imaged in every section of a series of 70 nm-thick ultrathin sections (n= 53 serial sections) using a scanning electron microscope. vGAT or PV-positive boutons were manually labeled throughout the series and quantified in 3D using stereological rules (red-green rectangle counting frame: exclusion and inclusion lines, respectively). A' and B': 3-dimensional view of all vGAT (A')- and PV-positive (B') boutons in the sampled volume. Every labeled bouton is indicated with a colored contour and a black dot in A' and B'. The bouton density of hippocampal layers was multiplied by the volume of the given layer for an estimation of the total number of vGAT or PV-positive boutons in the hippocampus. C-G: Estimation of the number of synapses/boutons. vGAT or PV-positive boutons were reconstructed in 3 dimensions from serial electron microscopic images (see Methods, D, G). Synapses are shown in red and

indicated with arrows in the 3D reconstructions. C, E, F: Synapses were identified by a parallel apposition of the pre-and postsynaptic membranes, a widening of the extracellular space at the presumptive synaptic cleft, and a postsynaptic membrane thickening. Arrowheads label the edges of synapses. In the human hippocampus, most of the vGAT and PV-positive boutons formed only one synapse (D, b1, b3, b4 in G) and only occasionally made two synapses (b3 in G). The scale bar in B' applies to A, A' and B, and scale bar in F applies to C, C' and E as well.

TABLES

Table 1. Estimated total number of PV, SOM, CR interneurons in one human hippocampal hemisphere (PV, CR: medians of three subjects, SOM: medians of two subjects)

PV	Volume [mm^3]	Abs. No
CA1 ori	39.17	**7041**
CA1 pyr	95.82	**13945**
CA1 rad	60.03	**1566**
CA1 lm	65.75	**769**
CA2 ori	15.62	**1494**
CA2 pyr	18.55	**2438**
CA2 rad	19.86	**0**
CA2 lm	13.18	**71**
CA3 ori	40.10	**725**
CA3 pyr	158.19	**9097**
CA3 rad	18.50	**132**
CA3 lm	4.73	**101**
DG mol	105.82	**1460**
DG gra	40.71	**3064**
DG hil	45.77	**3683**
Sum	**742**	**45586**

SOM	Volume [mm^3]	Abs. No
CA1 ori	37.33	**13101**
CA1 pyr	91.30	**24938**
CA1 rad	55.08	**2856**
CA1 lm	52.53	**707**
CA2 ori	14.46	**3801**
CA2 pyr	19.20	**3288**
CA2 rad	18.74	**689**
CA2 lm	9.68	**35**
CA3 ori	30.85	**9895**
CA3 pyr	120.28	**49887**
CA3 rad	13.24	**1385**
CA3 lm	3.74	**0**
DG mol	73.52	**377**
DG gra	31.88	**1458**
DG hil	33.76	**22079**
Sum	**606**	**134494**

CR	Volume [mm^3]	Abs. No
CA1 ori	39.17	**5972**
CA1 pyr	95.82	**22709**
CA1 rad	60.03	**48039**
CA1 lm	65.75	**36525**
CA2 ori	15.62	**1995**
CA2 pyr	18.55	**2138**
CA2 rad	19.86	**2148**
CA2 lm	13.18	**2759**
CA3 ori	40.10	**5709**
CA3 pyr	158.19	**16924**
CA3 rad	18.50	**4446**
CA3 lm	4.73	**1354**
DG mol	105.82	**21164**
DG gra	40.71	**28065**
DG hil	45.77	**28026**
Sum	**742**	**227974**

Table 2. Estimated total number of vGAT and PV-positive boutons and synapses in the human hippocampus, one hemisphere (data from SKO24)

Subregion	Layer	Volume (mm^3)	Labeling	Number of boutons/ 10^3 μm^3	Number of synapses/ 10^3 μm^3	Abs. No of boutons $*10^6$	Abs. No of synapses $*10^6$
CA1	ori	35.5	vGAT	8.55	9.26	303.4	328.7
			PV	0.22	0.24	7.8	8.5
	pyr	95.8	vGAT	37.58	45.09	3600.8	4321.0
			PV	16.44	19.72	1574.9	1889.9
	rad	50.1	vGAT	24.00	26.00	1202.7	1303.0
			PV	0.19	0.20	9.4	10.2
	l-m	65.8	vGAT	37.36	40.47	2456.4	2661.1
			PV	0.02	0.03	1.6	1.7
CA2	ori	13.3	vGAT	26.36	28.56	350.7	379.9
			PV	0.07	0.07	0.9	1.0
	pyr	18.5	vGAT	40.29	48.34	747.2	896.6
			PV	5.37	6.44	99.6	119.5
	rad	9.4	vGAT	38.16	41.34	357.0	386.8
			PV	0.19	0.20	1.7	1.9
	l-m	4.7	vGAT	49.52	53.65	234.4	253.9
			PV	0.04	0.04	0.2	0.2
CA3	ori	21.6	vGAT	22.39	24.25	483.5	523.8
			PV	0.10	0.11	2.2	2.4
	pyr	82.4	vGAT	27.57	33.09	2271.2	2725.5
			PV	4.75	5.70	391.4	469.6
	rad	8.0	vGAT	24.64	26.69	196.5	212.9
			PV	0.10	0.11	0.8	0.9
	l-m	2.8	vGAT	20.37	22.07	56.1	60.7
			PV	0.12	0.13	0.3	0.4
DG	mol	41.2	vGAT	64.62	67.43	2663.5	2779.3
			PV	0.06	0.06	2.3	2.4
	gra	23.1	vGAT	28.30	37.73	652.4	869.9
			PV	8.62	11.50	198.8	265.1
	hil	21.7	vGAT	21.47	22.40	466.9	487.2
			PV	0.20	0.21	4.5	4.6
SUM		**493.85**	vGAT			**16043**	**18190**
			PV			**2297**	**2778**

Supplementary tables for

Absolute number of three populations of interneurons and all GABAergic synapses in the human hippocampus

Virág Takács[1, #], Péter Papp[1, #], Áron Orosz[1,2], Zsuzsanna Bardóczi[1], Tamás Zsoldos[1], Masahiko Watanabe[3], Zsófia Maglóczky[4], Péter Gombás[5], Tamás F. Freund[1], Gábor Nyiri[1,*]

[#] These authors contributed equally.
*Corresponding author. Email: nyiri@koki.hu

Affiliations:
1) Laboratory of Cerebral Cortex Research, Institute of Experimental Medicine, Budapest, Hungary
2) János Szentágothai Doctoral School of Neurosciences, Semmelweis University, Budapest, Hungary
3) Department of Anatomy and Embryology, Hokkaido University, Sapporo, Japan
4) Human Brain Research Laboratory, Institute of Experimental Medicine, Budapest, Hungary
5) Department of Pathology, St. Borbála Hospital, Tatabánya, Hungary

Subject: SKO24, Immunohistochemistry: PV

Block	1		from 0 um - (Head)	2		from 8500 um -	3		from 20540 um -	4		from 25480 um -	Total		
SKO24 PV	Volume [mm³]	Density [cell/mm³]	Abs. No	Volume [mm³]	Density [cell/mm³]	Abs. No	Volume [mm³]	Density [cell/mm³]	Abs. No	Volume [mm³]	Density [cell/mm³]	Abs. No	Volume [mm³]	Density [cell/mm³]	Abs. No
CA1 ori	18.8	11.7	219.6	11.2	186.5	2080.2	5.1	287.6	1470.7	0.4	375.6	164.0	35.5	110.8	3934.5
CA1pyr	34.6	170.8	5906.9	24.6	176.2	4330.4	34.6	339.2	11728.7	2.1	430.1	900.0	95.8	238.6	22866.0
CA1 rad	18.2	8.9	162.8	12.3	18.8	230.4	18.2	62.4	1136.8	1.4	25.5	36.0	50.1	31.2	1566.0
CA1 lm	24.2	0.0	0.0	16.8	5.3	89.2	24.2	27.7	671.5	0.5	0.0	0.0	65.8	11.6	760.7
CA2 ori	3.9	0.0	0.0	5.1	234.4	1188.4	3.9	60.0	233.9	0.4	162.3	72.0	13.3	112.3	1494.2
CA2 pyr	5.0	71.4	360.0	7.6	117.0	889.8	5.0	192.8	972.2	0.9	251.6	216.0	18.5	131.4	2438.0
CA2 rad	2.1	0.0	0.0	4.7	0.0	0.0	2.1	0.0	0.0	0.5	0.0	0.0	9.4	0.0	0.0
CA2 lm	0.8	0.0	0.0	2.2	0.0	0.0	0.8	0.0	0.0	0.9	0.0	0.0	4.7	0.0	0.0
CA3 ori	4.6	9.8	45.6	10.8	16.2	175.3	4.6	61.5	285.2	1.5	23.4	36.0	21.6	25.1	542.1
CA3 pyr	19.7	37.1	730.6	40.1	59.6	2390.9	19.7	100.7	1982.1	2.9	125.0	360.0	82.4	66.3	5463.6
CA3 rad	1.2	0.0	0.0	5.0	0.0	0.0	1.2	37.5	44.6	0.6	0.0	0.0	8.0	5.6	44.6
CA3 lm	0.6	0.0	0.0	1.3	0.0	0.0	0.6	0.0	0.0	0.2	0.0	0.0	2.8	0.0	0.0
DG mol	6.8	0.0	0.0	26.3	4.2	110.7	6.8	14.1	95.8	1.3	0.0	0.0	41.2	5.0	206.5
DG gra	3.8	116.7	448.5	14.8	83.1	1232.9	3.8	293.1	1126.5	0.5	66.8	36.0	23.1	123.4	2843.8
DG hil	4.5	11.4	51.8	11.9	87.7	1042.0	4.5	289.2	1315.2	0.8	328.0	252.0	21.7	122.4	2661.0
Sum of all													493.9		44821.2

Subject: SKO24, Immunohistochemistry: SOM

Block	1		from 0 um - (Head)	2		from 8500 um -	3		from 20540 um -	4		from 25480 um -	Total		
SKO24 SOM	Volume [mm³]	Density [cell/mm³]	Abs. No	Volume [mm³]	Density [cell/mm³]	Abs. No	Volume [mm³]	Density [cell/mm³]	Abs. No	Volume [mm³]	Density [cell/mm³]	Abs. No	Volume [mm³]	Density [cell/mm³]	Abs. No
CA1 ori	18.8	410.8	7722.8	11.2	514.5	5738.4	5.1	587.5	3004.1	0.4	101.8	44.5	35.5	465.0	16509.8
CA1pyr	34.6	336.8	11647.2	24.6	362.5	8906.9	34.6	404.9	14000.5	2.1	367.8	769.6	95.8	368.6	35324.2
CA1 rad	18.2	90.0	1638.5	12.3	48.3	593.1	18.2	91.2	1661.6	1.4	50.2	71.0	50.1	79.1	3964.3
CA1 lm	24.2	15.6	377.3	16.8	8.9	149.5	24.2	33.1	801.8	0.5	0.0	0.0	65.8	20.2	1328.6
CA2 ori	3.9	577.1	2248.1	5.1	362.6	1838.1	3.9	173.2	674.7	0.4	506.4	224.7	13.3	374.8	4985.5
CA2 pyr	5.0	336.9	1698.9	7.6	109.6	833.7	5.0	146.9	740.6	0.9	70.5	60.5	18.5	179.7	3333.6
CA2 rad	2.1	212.0	435.2	4.7	82.0	388.6	2.1	32.0	65.7	0.5	0.0	0.0	9.4	95.1	889.6
CA2 lm	0.8	0.0	0.0	2.2	21.1	46.7	0.8	0.0	0.0	0.9	0.0	0.0	4.7	9.9	46.7
CA3 ori	4.6	322.1	1493.0	10.8	358.0	3862.1	4.6	370.7	1718.2	1.5	418.0	642.1	21.6	357.3	7715.4
CA3 pyr	19.7	493.2	9704.1	40.1	502.6	20177.5	19.7	557.7	10973.2	2.9	727.7	2095.7	82.4	521.4	42950.4
CA3 rad	1.2	86.9	103.4	5.0	74.3	370.3	1.2	249.5	296.9	0.6	0.0	0.0	8.0	96.6	770.6
CA3 lm	0.6	0.0	0.0	1.3	0.0	0.0	0.6	0.0	0.0	0.2	0.0	0.0	2.8	0.0	0.0
DG mol	6.8	0.0	0.0	26.3	12.8	338.3	6.8	26.7	180.5	1.3	14.2	19.0	41.2	13.0	537.7
DG gra	3.8	34.3	132.0	14.8	92.5	1372.2	3.8	73.5	282.6	0.5	0.0	0.0	23.1	77.5	1786.8
DG hil	4.5	543.9	2473.3	11.9	766.1	9105.1	4.5	1266.8	5761.0	0.8	1359.5	1044.6	21.7	845.3	18384.1
Sum of all													493.9		138527.4

Subject: SKO24, Immunohistochemistry: CR

Block	1		from 0 um - (Head)	2		from 8500 um -	3		from 20540 um -	4		from 25480 um -	Total		
SKO24 CR	Volume [mm³]	Density [cell/mm³]	Abs. No	Volume [mm³]	Density [cell/mm³]	Abs. No	Volume [mm³]	Density [cell/mm³]	Abs. No	Volume [mm³]	Density [cell/mm³]	Abs. No	Volume [mm³]	Density [cell/mm³]	Abs. No
CA1 ori	18.8	128.6	2417.9	11.2	246.2	2745.9	5.1	151.9	776.7	0.4	72.8	31.8	35.5	168.2	5972.3
CA1pyr	34.6	200.1	6917.3	24.6	261.0	6415.0	34.6	312.5	10805.7	2.1	423.3	885.7	95.8	261.2	25023.7
CA1 rad	18.2	305.1	5556.7	12.3	528.6	6490.7	18.2	755.8	13763.8	1.4	1841.3	2603.4	50.1	567.0	28414.6
CA1 lm	24.2	467.6	11336.8	16.8	438.1	7357.3	24.2	697.2	16903.6	0.5	1953.7	927.1	65.8	555.5	36524.8
CA2 ori	3.9	287.3	1119.2	5.1	122.2	619.5	3.9	38.7	150.8	0.4	237.5	105.4	13.3	150.0	1994.8
CA2 pyr	5.0	237.9	1199.4	7.6	144.9	1102.2	5.0	25.3	127.5	0.9	37.1	31.8	18.5	132.7	2460.9
CA2 rad	2.1	271.4	557.3	4.7	40.6	192.5	2.1	141.5	290.5	0.5	233.7	119.7	9.4	124.0	1160.1
CA2 lm	0.8	0.0	0.0	2.2	232.6	515.7	0.8	182.7	148.8	0.9	292.1	259.0	4.7	195.1	923.6
CA3 ori	4.6	142.9	662.1	10.8	203.8	2198.4	4.6	274.0	1269.8	1.5	332.2	510.3	21.6	214.9	4640.5
CA3 pyr	19.7	221.0	4347.9	40.1	155.1	6225.9	19.7	197.9	3893.6	2.9	351.5	1012.5	82.4	187.9	15479.9
CA3 rad	1.2	335.8	399.6	5.0	176.3	878.1	1.2	503.7	599.5	0.6	198.2	121.6	8.0	250.6	1998.8
CA3 lm	0.6	0.0	0.0	1.3	113.5	153.1	0.6	95.2	57.8	0.2	233.7	44.5	2.8	92.8	255.4
DG mol	6.8	396.8	2686.8	26.3	428.4	11283.5	6.8	372.4	2521.6	1.3	521.7	697.4	41.2	417.0	17189.4
DG gra	3.8	1042.8	4008.4	14.8	1184.7	17566.5	3.8	1332.0	5120.2	0.5	1733.0	933.7	23.1	1198.4	27628.9
DG hil	4.5	98.6	448.2	11.9	913.8	10860.0	4.5	1234.7	5615.3	0.8	1629.4	1252.0	21.7	835.7	18175.5
Sum of all													493.9		187843.2

Subject: SKO25, Immunohistochemistry: PV

Block	1	from 0 um - (Head)		2	from 7000 um -		3	from 18240 um -		4	from 29500 um -		5	from 38900 um -		Total		
SKO25 PV	Volume [mm³]	Density [cell/mm³]	Abs. No	Volume [mm³]	Density [cell/mm³]	Abs. No	Volume [mm³]	Density [cell/mm³]	Abs. No	Volume [mm³]	Density [cell/mm³]	Abs. No	Volume [mm³]	Density [cell/mm³]	Abs. No	Volume [mm³]	Density [cell/mm³]	Abs. No
CA1 ori	19.2	118.1	2263.7	8.0	246.2	1958.6	8.3	274.0	2284.5	2.0	169.3	338.5	1.7	115.0	195.5	39.2	179.8	7040.7
CA1pyr	42.4	37.0	1570.3	21.8	129.0	2806.6	15.0	181.9	2722.2	5.1	157.2	804.4	2.5	180.6	455.7	86.8	96.3	8359.3
CA1 rad	24.7	2.0	48.9	17.1	5.4	92.1	10.6	12.2	129.7	5.7	25.0	142.2	2.0	0.0	0.0	60.0	6.9	413.0
CA1 lm	11.2	11.1	125.0	14.1	13.9	195.7	8.3	47.0	388.2	4.4	0.0	0.0	1.4	43.3	59.8	39.3	19.6	768.6
CA2 ori	3.2	38.8	125.0	4.8	78.5	378.5	3.2	139.6	443.0	2.2	0.0	0.0	2.2	88.7	191.8	15.6	72.9	1138.3
CA2 pyr	4.3	58.1	250.0	6.2	123.3	760.2	4.4	165.9	724.6	2.7	141.1	375.1	2.4	195.0	459.0	19.9	129.4	2568.8
CA2 rad	7.2	0.0	0.0	9.7	0.0	0.0	5.7	0.0	0.0	2.9	0.0	0.0	2.7	0.0	0.0	28.1	0.0	0.0
CA2 lm	4.5	18.3	83.3	4.4	18.1	80.2	3.6	0.0	0.0	1.6	0.0	0.0	0.5	0.0	0.0	14.6	11.2	163.5
CA3 ori	0.0	0.0	0.0	13.4	8.1	107.7	16.6	17.6	293.6	4.9	55.5	270.5	5.2	10.3	53.6	40.1	18.1	725.4
CA3 pyr	29.6	22.5	666.7	48.5	28.6	1384.3	37.2	58.8	2187.1	25.4	97.1	2464.4	17.6	136.2	2394.4	158.2	57.5	9096.9
CA3 rad	0.0	0.0	0.0	9.3	28.9	268.8	6.4	0.0	0.0	2.0	0.0	0.0	0.8	0.0	0.0	18.5	14.5	268.8
CA3 lm	0.0	0.0	0.0	2.2	45.1	101.3	1.8	0.0	0.0	0.6	0.0	0.0	0.1	0.0	0.0	4.7	21.4	101.3
DG mol	16.0	10.4	166.7	27.9	5.4	151.9	30.5	16.1	490.9	18.5	31.7	587.5	12.9	36.7	473.5	105.8	17.7	1870.5
DG gra	6.5	57.3	375.0	9.5	37.2	352.6	13.5	81.8	1102.4	6.6	82.6	545.3	4.6	149.5	688.3	40.7	75.2	3063.5
DG hil	6.0	76.8	458.3	11.3	63.9	719.5	15.3	71.8	1101.8	5.9	169.5	1008.0	7.3	188.9	1373.0	45.8	101.8	4660.6
Sum of all																717.4		40239.2

Subject: SKO25, Immunohistochemistry: SOM

Block	1	from 0 um - (Head)		2	from 7000 um -		3	from 18240 um -		4	from 29500 um -		5	from 38900 um -		Total		
SKO25 SOM	Volume [mm³]	Density [cell/mm³]	Abs. No	Volume [mm³]	Density [cell/mm³]	Abs. No	Volume [mm³]	Density [cell/mm³]	Abs. No	Volume [mm³]	Density [cell/mm³]	Abs. No	Volume [mm³]	Density [cell/mm³]	Abs. No	Volume [mm³]	Density [cell/mm³]	Abs. No
CA1 ori	19.2	243.5	4668.0	8.0	127.8	1016.7	8.3	375.6	3131.2	2.0	402.3	804.1	1.7	42.1	71.6	39.2	247.5	9691.5
CA1pyr	42.4	65.9	2794.8	21.8	260.2	5661.2	15.0	304.9	4564.0	5.1	257.0	1315.2	2.5	85.6	215.9	86.8	167.7	14551.1
CA1 rad	24.7	20.6	507.9	17.1	28.7	490.1	10.6	59.0	625.6	5.7	21.9	124.5	2.0	0.0	0.0	60.0	29.1	1748.1
CA1 lm	11.2	0.0	0.0	14.1	6.0	85.1	8.3	0.0	0.0	4.4	0.0	0.0	1.4	0.0	0.0	39.3	2.2	85.1
CA2 ori	3.2	110.1	354.4	4.8	121.2	584.8	3.2	137.7	436.9	2.2	101.2	227.1	2.2	468.9	1013.7	15.6	167.5	2617.0
CA2 pyr	4.3	111.2	478.8	6.2	182.7	1126.5	4.4	185.5	809.9	2.7	226.9	603.4	2.4	94.8	223.0	19.9	163.3	3241.7
CA2 rad	7.2	36.9	264.5	9.7	9.3	90.1	5.7	0.0	0.0	2.9	0.0	0.0	2.7	50.3	134.1	28.1	17.4	488.7
CA2 lm	4.5	5.0	22.7	4.4	0.0	0.0	3.6	0.0	0.0	1.6	0.0	0.0	0.5	0.0	0.0	14.6	1.5	22.7
CA3 ori	0.0	453.1	0.0	13.4	322.6	4314.1	16.6	282.4	4700.5	4.9	231.2	1127.7	5.2	371.2	1932.2	40.1	301.1	12074.4
CA3 pyr	29.6	480.4	14203.5	48.5	377.9	18321.3	37.2	296.2	11012.0	25.4	263.2	6682.9	17.6	375.6	6604.5	158.2	359.2	56824.2
CA3 rad	0.0	0.0	0.0	9.3	120.5	1119.5	6.4	64.9	416.0	2.0	19.6	38.9	0.8	517.4	424.3	18.5	108.0	1998.7
CA3 lm	0.0	0.0	0.0	2.2	0.0	0.0	1.8	0.0	0.0	0.6	0.0	0.0	0.1	0.0	0.0	4.7	0.0	0.0
DG mol	16.0	5.2	83.1	27.9	2.6	73.8	30.5	1.9	59.1	18.5	0.0	0.0	12.9	0.0	0.0	105.8	2.0	216.1
DG gra	6.5	26.2	171.6	9.5	31.2	296.2	13.5	28.7	386.5	6.6	33.7	222.4	4.6	11.3	52.1	40.7	27.7	1128.8
DG hil	6.0	276.8	1650.8	11.3	439.4	4944.0	15.3	477.3	7323.5	5.9	597.2	3551.8	7.3	1142.6	8303.1	45.8	563.1	25773.2
Sum of all																717.4		130461.2

Subject: SKO25, Immunohistochemistry: CR

Block	1	from 0 um - (Head)		2	from 7000 um -		3	from 18240 um -		4	from 29500 um -		5	from 38900 um -		Total		
SKO25 CR	Volume [mm³]	Density [cell/mm³]	Abs. No	Volume [mm³]	Density [cell/mm³]	Abs. No	Volume [mm³]	Density [cell/mm³]	Abs. No	Volume [mm³]	Density [cell/mm³]	Abs. No	Volume [mm³]	Density [cell/mm³]	Abs. No	Volume [mm³]	Density [cell/mm³]	Abs. No
CA1 ori	19.2	40.7	780.3	8.0	70.6	561.7	8.3	101.9	849.9	2.0	130.9	261.7	1.7	159.2	270.6	39.2	69.6	2724.1
CA1pyr	42.4	226.4	9606.3	21.8	285.9	6219.5	15.0	191.9	2872.5	5.1	217.4	1112.8	2.5	69.1	174.5	86.8	230.3	19985.5
CA1 rad	24.7	688.5	16987.8	17.1	833.9	14223.9	10.6	1138.6	12062.0	5.7	1024.5	5823.8	2.0	294.6	596.5	60.0	827.8	49694.0
CA1 lm	11.2	484.2	5434.8	14.1	547.9	7717.7	8.3	420.4	3474.4	4.4	309.4	1348.4	1.4	123.5	170.5	39.3	461.6	18145.8
CA2 ori	3.2	37.2	119.8	4.8	53.9	259.9	3.2	55.6	176.5	2.2	120.4	270.1	2.2	181.8	392.9	15.6	78.0	1219.2
CA2 pyr	4.3	150.4	647.7	6.2	96.6	595.5	4.4	90.9	396.8	2.7	90.9	241.7	2.4	109.1	256.8	19.9	107.7	2138.4
CA2 rad	7.2	228.7	1639.0	9.7	61.4	596.3	5.7	153.2	869.6	2.9	192.4	558.9	2.7	276.2	736.8	28.1	156.5	4400.5
CA2 lm	4.5	509.5	2315.4	4.4	177.4	785.1	3.6	215.9	774.5	1.6	190.2	296.2	0.5	71.1	36.4	14.6	287.6	4207.6
CA3 ori	0.0	34.5	0.0	13.4	75.0	1003.0	16.6	148.7	2474.7	4.9	99.8	486.9	5.2	335.1	1744.3	40.1	142.4	5708.9
CA3 pyr	29.6	96.0	2837.5	48.5	75.4	3656.9	37.2	166.3	6183.0	25.4	170.4	4326.1	17.6	261.3	4595.3	158.2	136.5	21598.8
CA3 rad	0.0	0.0	0.0	9.3	174.9	1625.0	6.4	288.1	1845.3	2.0	153.3	304.8	0.8	818.2	671.0	18.5	240.3	4446.1
CA3 lm	0.0	0.0	0.0	2.2	84.5	189.8	1.8	484.7	879.8	0.6	372.9	227.9	0.1	935.1	56.9	4.7	286.1	1354.3
DG mol	16.0	173.2	2769.1	27.9	292.9	8185.1	30.5	297.7	9072.4	18.5	308.3	5710.5	12.9	331.5	4272.5	105.8	283.6	30009.6
DG gra	6.5	315.8	2065.1	9.5	345.7	3278.4	13.5	993.7	13396.7	6.6	767.0	5063.3	4.6	925.3	4261.2	40.7	689.3	28064.7
DG hil	6.0	303.6	1811.1	11.3	531.1	5976.2	15.3	1150.0	17644.5	5.9	1086.5	6462.0	7.3	943.6	6857.0	45.8	846.6	38750.7
Sum of all																717.4		232448.0

Subject: SKO27, Immunohistochemistry: PV

Block	1	from 0 um - (Head)		2	from 3980 um -		3	from 12580 um -		4	from 22180 um -		5	from 31960 um -		Total		
SKO27 PV	Volume [mm³]	Density [cell/mm³]	Abs. No	Volume [mm³]	Density [cell/mm³]	Abs. No	Volume [mm³]	Density [cell/mm³]	Abs. No	Volume [mm³]	Density [cell/mm³]	Abs. No	Volume [mm³]	Density [cell/mm³]	Abs. No	Volume [mm³]	Density [cell/mm³]	Abs. No
CA1 ori	18.5	66.8	1233.5	13.3	105.8	1406.4	10.4	135.2	1408.9	13.0	177.5	2308.7	9.8	322.9	3151.1	64.9	146.4	9508.7
CA1pyr	37.6	54.9	2066.6	42.3	74.1	3130.1	19.0	111.1	2110.4	20.1	110.4	2214.8	27.5	160.8	4423.3	146.4	95.2	13945.2
CA1 rad	23.0	0.0	0.0	17.1	4.8	81.6	19.6	59.1	1161.6	15.4	24.6	378.3	14.8	51.1	756.1	89.9	26.5	2377.5
CA1 lm	32.7	3.1	100.3	16.9	2.7	45.5	7.3	57.4	418.8	10.2	39.5	403.7	11.2	334.6	3731.3	78.2	60.1	4699.5
CA2 ori	5.9	41.5	244.7	4.2	95.4	401.0	2.0	149.1	300.8	3.5	137.7	488.5	0.9	100.7	89.2	16.6	92.1	1524.3
CA2 pyr	4.3	94.3	402.6	5.3	88.1	463.9	2.3	235.3	541.1	2.9	171.1	502.0	1.6	216.3	356.7	16.4	138.0	2266.2
CA2 rad	5.2	0.0	0.0	7.7	0.0	0.0	2.9	0.0	0.0	2.5	0.0	0.0	1.5	0.0	0.0	19.9	0.0	0.0
CA2 lm	3.4	8.1	27.8	3.9	0.0	0.0	1.5	0.0	0.0	2.3	0.0	0.0	2.0	21.8	42.7	13.2	5.4	70.6
CA3 ori	7.1	6.9	49.6	14.9	24.5	365.4	14.1	23.7	335.1	8.9	108.0	959.8	10.7	60.8	649.5	55.8	42.3	2359.4
CA3 pyr	27.3	49.1	1340.2	77.7	31.7	2461.6	32.5	40.8	1326.4	28.7	55.3	1584.8	25.0	117.0	2927.9	191.2	50.4	9640.9
CA3 rad	10.3	5.2	53.4	9.9	3.5	34.2	8.0	0.0	0.0	3.7	0.0	0.0	3.4	13.2	44.4	35.2	3.8	132.0
CA3 lm	2.4	10.5	24.8	4.4	8.2	35.8	1.9	0.0	0.0	1.2	0.0	0.0	1.7	24.9	42.2	11.6	8.9	102.8
DG mol	30.4	12.3	375.2	41.0	2.5	104.1	32.8	15.1	496.9	26.0	8.5	220.4	27.9	9.4	263.1	158.2	9.2	1459.7
DG gra	9.5	67.3	638.8	44.6	6.3	279.6	10.1	20.9	210.4	11.4	165.8	1893.2	7.5	196.8	1479.8	83.1	54.2	4501.8
DG hil	10.7	18.2	194.4	15.1	33.3	503.3	9.6	67.8	651.9	12.1	102.2	1238.7	8.1	135.5	1095.1	55.7	66.2	3683.4
Sum of all																1036.2		56271.9

Subject: SKO27, Immunohistochemistry: SOM

Block	1	from 0 um - (Head)		2	from 3980 um -		3	from 12580 um -		4	from 22180 um -		5	from 31960 um -		Total		
SKO27 SOM	Volume [mm³]	Density [cell/mm³]	Abs. No	Volume [mm³]	Density [cell/mm³]	Abs. No	Volume [mm³]	Density [cell/mm³]	Abs. No	Volume [mm³]	Density [cell/mm³]	Abs. No	Volume [mm³]	Density [cell/mm³]	Abs. No	Volume [mm³]	Density [cell/mm³]	Abs. No
CA1 ori	18.5	281.8	5203.2	13.3	35.2	468.5	10.4	157.2	1638.3	13.0	135.9	1767.9	9.8	25.2	246.2	64.9	143.6	9324.1
CA1pyr	37.6	55.2	2074.9	42.3	5.7	241.2	19.0	20.1	382.7	20.1	22.0	441.5	27.5	31.2	857.2	146.4	27.3	3997.6
CA1 rad	23.0	37.6	863.3	17.1	0.0	0.0	19.6	7.0	138.3	15.4	14.0	215.5	14.8	0.0	0.0	89.9	13.5	1217.1
CA1 lm	32.7	3.9	128.1	16.9	0.0	0.0	7.3	0.0	0.0	10.2	0.0	0.0	11.2	0.0	0.0	78.2	1.6	128.1
CA2 ori	5.9	394.4	2327.3	4.2	40.9	171.9	2.0	90.7	183.0	3.5	156.0	553.7	0.9	115.4	102.2	16.6	201.6	3338.1
CA2 pyr	4.3	61.7	263.4	5.3	21.8	114.8	2.3	65.7	151.1	2.9	40.4	118.6	1.6	76.9	126.8	16.4	47.2	774.7
CA2 rad	5.2	12.1	63.1	7.7	0.0	0.0	2.9	0.0	0.0	2.5	0.0	0.0	1.5	55.5	84.1	19.9	7.4	147.2
CA2 lm	3.4	0.0	0.0	3.9	0.0	0.0	1.5	0.0	0.0	2.3	0.0	0.0	2.0	0.0	0.0	13.2	0.0	0.0
CA3 ori	7.1	154.4	1102.6	14.9	25.2	376.4	14.1	155.2	2193.5	8.9	161.4	1435.1	10.7	101.1	1080.3	55.8	110.9	6187.9
CA3 pyr	27.3	214.6	5851.4	77.7	58.3	4532.5	32.5	116.5	3787.3	28.7	234.5	6726.4	25.0	344.0	8607.6	191.2	154.3	29505.2
CA3 rad	10.3	112.4	1156.2	9.9	14.5	142.6	8.0	33.2	266.2	3.7	54.7	201.0	3.4	0.0	0.0	35.2	50.2	1766.0
CA3 lm	2.4	58.5	138.5	4.4	20.3	88.6	1.9	0.0	0.0	1.2	0.0	0.0	1.7	0.0	0.0	11.6	19.6	227.1
DG mol	30.4	2.0	59.5	41.0	2.0	83.9	32.8	0.0	0.0	26.0	1.7	45.5	27.9	0.0	0.0	158.2	1.2	188.9
DG gra	9.5	30.1	285.3	44.6	9.2	412.3	10.1	0.0	0.0	11.4	21.5	245.9	7.5	0.0	0.0	83.1	11.4	943.5
DG hil	10.7	183.9	1968.4	15.1	64.1	969.0	9.6	240.3	2311.6	12.1	163.1	1977.0	8.1	170.5	1377.5	55.7	154.6	8603.5
Sum of all																1036.2		66349.2

Subject: SKO27, Immunohistochemistry: CR

Block	1	from 0 um - (Head)		2	from 3980 um -		3	from 12580 um -		4	from 22180 um -		5	from 31960 um -		Total		
SKO27 CR	Volume [mm³]	Density [cell/mm³]	Abs. No	Volume [mm³]	Density [cell/mm³]	Abs. No	Volume [mm³]	Density [cell/mm³]	Abs. No	Volume [mm³]	Density [cell/mm³]	Abs. No	Volume [mm³]	Density [cell/mm³]	Abs. No	Volume [mm³]	Density [cell/mm³]	Abs. No
CA1 ori	18.5	177.1	3270.0	13.3	89.5	1189.4	10.4	47.6	495.8	13.0	97.2	1264.0	9.8	115.7	1129.1	64.9	113.2	7348.3
CA1pyr	37.6	128.9	4847.8	42.3	140.1	5921.4	19.0	94.3	1791.8	20.1	162.2	3253.1	27.5	250.6	6894.9	146.4	155.1	22709.0
CA1 rad	23.0	290.2	6671.5	17.1	337.0	5757.3	19.6	326.8	6417.7	15.4	592.2	9109.5	14.8	1357.7	20083.1	89.9	534.5	48039.1
CA1 lm	32.7	773.7	25284.2	16.9	566.6	9564.7	7.3	391.4	2855.7	10.2	320.7	3278.0	11.2	389.0	4337.6	78.2	579.3	45320.2
CA2 ori	5.9	393.1	2319.6	4.2	191.3	804.3	2.0	50.0	100.8	3.5	83.5	296.4	0.9	85.9	76.1	16.6	217.3	3597.1
CA2 pyr	4.3	321.6	1372.6	5.3	42.6	224.4	2.3	42.0	96.6	2.9	23.7	69.6	1.6	20.0	33.0	16.4	109.4	1796.2
CA2 rad	5.2	161.9	842.5	7.7	86.7	664.7	2.9	110.6	323.1	2.5	45.1	115.0	1.5	133.8	202.7	19.9	108.2	2148.1
CA2 lm	3.4	361.9	1243.5	3.9	290.4	1141.9	1.5	99.7	150.4	2.3	0.0	0.0	2.0	114.1	223.6	13.2	209.3	2759.4
CA3 ori	7.1	120.4	859.5	14.9	190.7	2847.9	14.1	25.4	359.4	8.9	77.3	687.7	10.7	127.3	1361.0	55.8	109.6	6115.5
CA3 pyr	27.3	164.1	4474.2	77.7	48.7	3786.5	32.5	18.6	604.2	28.7	104.0	2983.3	25.0	202.8	5076.0	191.2	88.5	16924.1
CA3 rad	10.3	215.3	2215.4	9.9	134.4	1325.0	8.0	50.2	402.2	3.7	85.3	313.6	3.4	93.6	314.2	35.2	129.9	4570.4
CA3 lm	2.4	286.9	679.3	4.4	167.6	732.1	1.9	0.0	0.0	1.2	0.0	0.0	1.7	174.2	294.7	11.6	147.5	1706.1
DG mol	30.4	125.8	3824.0	41.0	116.5	4779.6	32.8	94.5	3104.9	26.0	132.0	3436.7	27.9	215.8	6019.2	158.2	133.8	21164.4
DG gra	9.5	233.1	2211.7	44.6	313.1	13963.0	10.1	301.7	3039.6	11.4	473.0	5401.5	7.5	1017.4	7649.3	83.1	388.3	32265.1
DG hil	10.7	343.6	3677.6	15.1	397.1	6007.6	9.6	394.2	3791.0	12.1	606.3	7350.2	8.1	891.2	7199.7	55.7	503.6	28026.1
Sum of all																1036.2		244489.2